PALACKÝ UNIVERSITY
FACULTY OF NATURAL SCIENCES

MASTER'S THESIS

Construction and characterization of a three-photon source

Joint Laboratory of Optics of Palacký University and the Institute of Physics of Czech Academy of Sciences

Author:	Vojtěch Trávníček
Supervisor:	doc. Mgr. Karel Lemr, Ph.D.
Field of study:	Nanotechnology
Form of study:	Full-time
Defended in:	2017
Guaranteed by:	Department of Experimental physics, Faculty of Science

Bibliografical details

Author's first name and surname:	Vojtěch Trávníček
Title:	Construction and characterization of a three-photon source
Type of thesis:	Master's
Workplace:	Joint Laboratory of Optics of Palacký University and the Institute of Physics of Czech Academy of Sciences
Guaranteed by:	Department of Experimental physics, Faculty of Science
Supervisor:	doc. Mgr. Karel Lemr, Ph.D.
Defended in:	2017
Number of pages:	49
Language:	English

Declaration of originality

I hereby declare that this thesis is my own work and that, to the best of my knowledge and belief, it contains no material previously published or written by another person nor material which to a substantial extent has been accepted for the award of any other degree or diploma of the university or other institute of higher learning, except where due acknowledgement has been made in the text.

Olomouc, ..., 2016 . . . .

The author grants permission to Palacký University in Olomouc to store and display this thesis and its electronic version in university library and on official website.

Acknowledgement

I would like to express my sincere gratitude to my supervisor doc. Mgr. Karel Lemr, Ph.D., for patient guidance and to Mgr. Antonín Černoch, Ph.D., for irreplaceable help in the laboratory. My thanks also belong to co-authors of our publication Karol Bartkiewicz, Antonín Černoch and Karel Lemr.

Abstract

In this thesis, we develop a simple model describing inherent photon-number noise in Rarity-Tapster type interferometers. This noise is caused by generating photon pairs in the process of spontaneous parametric down-conversion and adding a third photon by attenuating fundamental laser mode to single-photon level. We experimentally verify our model and present resulting signal to noise ratios as well as obtained three-photon generation rates as functions of various setup parameters. Subsequently we evaluate impact of this particular source of noise on quantum teleportation which is a key quantum information protocol using this interferometric configuration. Finally, we test our model on simple case of Hong-Ou-Mandel interference.

Contents

1 Introduction **3**

1.1 Quantum physics . . . 3

1.2 Motivation for our work . . . 4

2 Methods and tools **7**

2.1 Quantization of the electromagnetic field . . . 7

2.2 Fock states . . . 9

2.3 Coherent state . . . 10

2.4 Qubit . . . 11

2.5 Spontaneous parametric down-conversion . . . 13

2.5.1 Type I . . . 14

2.5.2 Type II . . . 15

2.5.3 The Kwiat source of entangled photons . . . 16

2.6 Beam splitter . . . 17

3 Theoretical model **21**

4 Experiment **27**

4.1 Impact of the noise on teleportation fidelity . . . 33

5 Hong-Ou-Mandel interference **37**

6 Conclusions **41**

7 Appendix **49**

1 Introduction

1.1 Quantum physics

During the 19th century, physicists observed phenomena which could not be explained by means of classical physics (characteristic x-ray radiation, photoelectric effect). This crysis of classical physics culminated at the beginnig of the 20th century when Max Planck, in an effort to explain the black body radiation, concluded that the spectrum can be clarified only if we assume that the black body and electromagnetic field exchange energy in quanta [1]. Later, the same assumption was used by Albert Einstein to explain the theory of photoelectric effect [2]. The idea of non–continuous energy transfer led to a revolution in physics and explanations of phenomena unsolvable by classical physics. Since then, physicists began to build the most advanced theory we know to this day, the quantum theory [3].

Key principles of the quantum theory are the superposition and the entanglement. Quantum superposition principle states that if two or more quantum states are solutions to the Schrödinger equation then also any linear combination of the states is a solution. Quantum entanglement, or non-locality, occurs when a pair or a group of particles is generated or interact in such way that quantum state of individual particle can not be described independently of the others [3]. Quantum entanglement in fact causes correlation, so for example if one creates two photons simultaneously with one photon being polarized horizontally the other vertically and we can not tell them apart, they become entangled and we can write the state of the system as

$$|\psi\rangle = \frac{1}{\sqrt{2}}(|HV\rangle - |VH\rangle). \tag{1.1}$$

Note that the state of the system can be expressed as a superposition of individual states. This means that if we do a measurement and we observe the first photon being polarized horizontally, the other must be polarized vertically and vice versa. So far, the classical interpretation allows to explain this type of correlation. However, consider detecting (projecting) one of the photons in a diagonal linear polarization state ($|D\rangle = \frac{1}{\sqrt{2}}(|H\rangle + |V\rangle)$). The other will be found in an anti-diagonally polarized state ($|A\rangle = \frac{1}{\sqrt{2}}(|H\rangle - |V\rangle)$). Classical physics fails to explain this effect.

Entanglement and superposition are the key components for quantum information processing including quantum computing and quantum communications. The advantages of the quantum way are for example faster algorithms [4, 5] enabling quantum computer to solve some calculations much faster or quantum cryptography which is a method for secure information transfer relying on quantum laws of nature [6, 7].

1.2 Motivation for our work

Quantum information processing (QIP) is a modern and perspective reaserch discipline of information science [8–10]. One of the platforms suitable for QIP are discrete photons manipulated using linear optics [11]. This platform is particularly promising for quantum communications, because of fast and relatively noiseless propagation of individual photons through open space or in fibers [12, 13].

Quantum teleportation [14, 15] is a key ingredient for many quantum information protocols such as entanglement swapping [16], quantum relays [17] or teleportation-based quantum computing [18]. On the platform of linear optics, quantum teleportation is usually achieved in the so-called Rarity-Tapster interferometer [19] (shown in Fig. 4.1). In this interferometer, one photon from an entangled pair gets overlapped on a balanced beam splitter with an independent photon [11]. The output ports of the beam splitter are then subjected to suitable Bell-state projection.

Single–photon sources used in experimental quantum information processing today are however imperfect and the number of photons generated per pulse is random, given by the state's photopulse statistics (e.g. Bose-Einstein, Poisson). While vacuum states can be filtered out by suitable post-selection, higher photon-number contributions can not always be recognized [20, 21].

In this thesis, we develop a simple model describing inherent photon-number noise in Rarity-Tapster type interferometers based on sources using spontaneous parametric down conversion (SPDC) and attenuated coherent state. These are currently predominant photon sources in experimental linear-optical QIP [12, 22–27]. We have experimentally tested validity of our model and established both theoretical and experimental relations between photon-number noise and various setup parameters. Our goal was also to quantify the effect of photon-number noise on teleportation fidelity. Photon-number noise does not originate from experimental imperfections but is rather an intrinsic property of various photon sources. This fact even further stresses out the importance of this investigation. To our best knowledge an article on this topic have not yet been published and can be higly beneficial to future research in linear–optical QIP.

2 Methods and tools

2.1 Quantization of the electromagnetic field

First of all we should describe the electromagnetic field by means of the quantum theory. It will be usefull for subsequent description of quantum–optical tools that we use in our experiment. We start from Maxwell's equations for electromagnetic field in vacuum [28]

$$\nabla \cdot \vec{B} = 0 \tag{2.1}$$

$$\nabla \cdot \vec{D} = 0 \tag{2.2}$$

$$\nabla \times \vec{E} = -\frac{\partial \vec{B}}{\partial t} \tag{2.3}$$

$$\nabla \times \vec{H} = \frac{\partial \vec{D}}{\partial t}, \tag{2.4}$$

where $\vec{B} = \mu_0 \vec{H}$, $\vec{D} = \varepsilon_0 \vec{E}$ and $\mu_0 \epsilon_0 = 1/c^2$. Using the Coulomb gauge, the $\vec{E}$ and $\vec{B}$ are then determined by the vector potential $\vec{A}$

$$\vec{B} = \nabla \times \vec{A} \tag{2.5}$$

$$\vec{E} = -\frac{\partial \vec{A}}{\partial t}, \tag{2.6}$$

and with the Coulomb gauge condition

$$\nabla \cdot \vec{A} = 0 \tag{2.7}$$

one can express the wave equation for $\vec{A}$ as

$$\nabla^2 A(r,t) = \frac{1}{c^2} \frac{\partial^2 A(r,t)}{\partial^2 t}. \tag{2.8}$$

The function $A(r,t)$ can be decomposed as

$$A(r,t) = -i\sum_{k=1}^{\infty}\sqrt{\frac{\hbar}{2\omega_k\varepsilon_0}}[u_k(r)a_k(t) + u_k^*(r)a_k^*(t)], \tag{2.9}$$

solving the wave equation 2.8 gives us

$$a_k(t) = a_k e^{-i\omega_k t}. \tag{2.10}$$

Now we have to find solution for $u_k(r)$. The solution can be either sinusoidal (wave in optical cavity) or exponential (free wave). Considering periodic boundary conditions

$$u_k(r) = u_k(r + Lx) = u_k(r + Ly) = u_k(r + Lz) \tag{2.11}$$

one finds that

$$u_k(r) = \epsilon_k \frac{1}{\sqrt{V}} e^{ik_n r}, \tag{2.12}$$

where $V = L^3$, $k_n = 2\pi/L$ and ϵ_k is polarization vector.

Therefore

$$A(r,t) = -i\sum_{k=1}^{\infty}\sqrt{\frac{\hbar}{2\omega_k\varepsilon_0 V}}\epsilon_k[a_k e^{-i\omega_k t + ik_n r} + c.c.] \tag{2.13}$$

$$E(r,t) = \sum_{k=1}^{\infty}\sqrt{\frac{\hbar\omega_k}{2\varepsilon_0 V}}\epsilon_k[a_k e^{-i\omega_k t + ik_n r} + c.c.] \tag{2.14}$$

$$H(r,t) = \frac{1}{\mu_0}\sum_{k=1}^{\infty}\sqrt{\frac{\hbar\omega_k}{2\varepsilon_0 V}}(k_n \times \epsilon_k)[a_k e^{-i\omega_k t + ik_n r} + c.c.], \tag{2.15}$$

where normalization constant

$$E_0 = \sqrt{\frac{\hbar\omega_k}{2\varepsilon_0 V}} \tag{2.16}$$

is the electric field per photon.

Because the a_k,a_k^* folow the equations of motion of a harmonic oscillator, the quantization can be easily obtained by replacing the complex numbers with operators

$$a \to \hat{a} \tag{2.17}$$

$$a^* \to \hat{a}^\dagger, \tag{2.18}$$

called the annihilation and creation operators. Their commutation relations are

$$[\hat{a}_m, \hat{a}_n^+] = \delta_{mn} \tag{2.19}$$

$$[\hat{a}_m, \hat{a}_n] = 0 \tag{2.20}$$

$$[\hat{a}_m^+, \hat{a}_n^+] = 0. \tag{2.21}$$

The Hamiltonian for the quantized electromagnetic field reads

$$H = \sum_{k=1}^{\infty} \hbar\omega_k (\hat{a}_k^+ \hat{a}_k + 1/2) \tag{2.22}$$

or with the indroduction of number oparator

$$\hat{n}_k = \hat{a}_k^+ \hat{a}_k \tag{2.23}$$

$$H = \sum_{k=1}^{\infty} \hbar\omega_k (\hat{n}_k + 1/2). \tag{2.24}$$

2.2 Fock states

Fock states are eigenstates of the number oparator $\hat{n}_k$ [29]

$$\hat{n}_k |n_k\rangle = n_k |n_k\rangle. \tag{2.25}$$

The operators $\hat{a}_k$ and $\hat{a}_k^\dagger$ are known as the anihilation and creation operators with subsequent properties

$$\hat{a}_k |n_k\rangle = \sqrt{n_k} |n_k - 1\rangle \tag{2.26}$$

$$\hat{a}_k^\dagger |n_k\rangle = \sqrt{n_k + 1} |n_k + 1\rangle, \tag{2.27}$$

therefore

$$|n_k\rangle = \frac{(\hat{a}_k^\dagger)^{n_k}}{(n_k!)^{1/2}} |0\rangle, \tag{2.28}$$

with $|0\rangle$ being the vacuum state.

2.3 Coherent state

Coherent state of a mode of elecromagnetic field is defined as eigenstate of the annihilation oparator [30]

$$\hat{a}|\alpha\rangle = \alpha|\alpha\rangle. \tag{2.29}$$

Coherent state, just like any other state, can be expressed as a superposition of Fock states

$$|\alpha\rangle = \sum_{n=0}^{\infty}\langle n|\alpha\rangle|n\rangle, \tag{2.30}$$

where $|n\rangle$ is the Fock state which satisfies the equation

$$|n\rangle = \frac{1}{\sqrt{n!}}(\hat{a}^{\dagger})^n|0\rangle. \tag{2.31}$$

To evaluate the term $\langle n|\alpha\rangle$, we need to take the Hermitian conjugate of the Fock state and perform a scalar product with the coherent state $|\alpha\rangle$. The Eq.(2.30) then takes the form of

$$|\alpha\rangle = \sum_{n=0}^{\infty}\frac{1}{\sqrt{n!}}\alpha^n\langle 0|\alpha\rangle|n\rangle, \tag{2.32}$$

where the term $\langle 0|\alpha\rangle$ is yet to be determined. In regart to the fact that scalar product $\langle\alpha|\alpha\rangle$ is one, the folowing equation is derived from normalization

$$|\langle 0|\alpha\rangle|^2 = \mathrm{e}^{-|\alpha|^2}. \tag{2.33}$$

Let us choose the phase of the scalar product $\langle 0|\alpha\rangle$ to be zero, the expansion of the coherent state into Fock basis then reads

$$|\alpha\rangle = \sum_{n=0}^{\infty}\frac{1}{\sqrt{n!}}\alpha^n\mathrm{e}^{-\frac{|\alpha|^2}{2}}|n\rangle. \tag{2.34}$$

Using the Eg. (2.34), we can easily derive the probability amplitude in the form of

$$\langle n|\alpha\rangle = \frac{1}{\sqrt{n!}}\alpha^n\mathrm{e}^{-\frac{|\alpha|^2}{2}}, \tag{2.35}$$

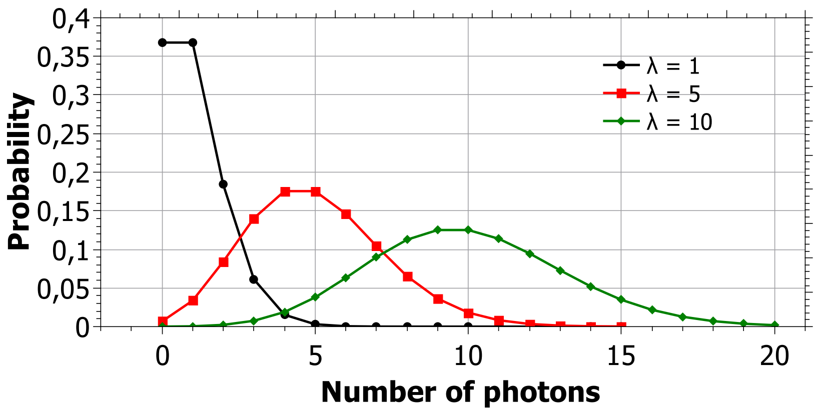

Figure 2.1: Graph shows several Poisson distributions where λ is the expected number of occurrences.

then the probability of a coherent state to contain defined number of photons n or energy $E = hf(n + 1/2)$ is

$$p(n) = |\langle n|\alpha\rangle|^2 = \frac{1}{n!}|\alpha|^2 n e^{-|\alpha|^2}. \tag{2.36}$$

The derived probability distribution is known as Poisson distribution (see Fig. 2.1). It is obvious that electromagnetic field in coherent state does not have exactly defined number of photons (energy). The result of an energy measurement is a Poisson distribution function with mean value and variance equal to the quadrature of complex number α.

2.4 Qubit

Qubit is a basic unit of information used in quantum computing. It's analogy in classical information science is a bit. Bit is a two state system which value can be typically either 0 or 1. Qubit is in some way similar to the bit but in some properties the two differ. Just as the bit, the qubit is a two state system and measurement on this system yields two possible outcomes usually 0 and 1. The difference is that whereas the bit can be only in the state 0 or 1 [31], the state of the qubit can also be a superposition of both [e.g. $1/\sqrt{13}(3|0\rangle + 2|1\rangle)$] [32]. The term qubit was first mentioned by B. Schumacher [33].

Qubit is formally defined as normalized vector in a two-dimensional Hilbert space. Let us denote $\mathcal{H}$ the two-dimensional Hilber space with ortonormal basis $|0\rangle, |1\rangle$, then element $|\psi\rangle \in \mathcal{H}$ of the vector space with a unit size is the qubit. Therefore qubit is a vector

$$|\psi\rangle = \alpha|0\rangle + \beta|1\rangle, \tag{2.37}$$

where $\alpha, \beta \in \mathbb{C}$ are the coordinates of the vector in the basis $|0\rangle, |1\rangle$, The α and β parameters are also called probability amplitudes, that must match the normalization constraint $|\alpha|^2 + |\beta|^2 = 1$. The quadratures of the probability amplitudes are then interpreted as probabilities of finding state $|\psi\rangle$ in the state $|0\rangle$ or $|1\rangle$.

Qubit can be represented by any two–level quantum system such as an electron in the atom or the polarization of a photon. The photon can be prepared in such way that its polarization is in superposition of basis states so it can store quantum information [34–36]. It is useful to visualise polarization states using the Bloch sphere (see Fig.2.2) where horizontal and vertical polarization (logical state $|0\rangle$ and $|1\rangle$) sit on the poles, meanwhile their balanced superpositions are situated on the equator. The advantage of photons is that they are fast and resisitant to decoherence which makes them suitable for quantum information processing (QIP).

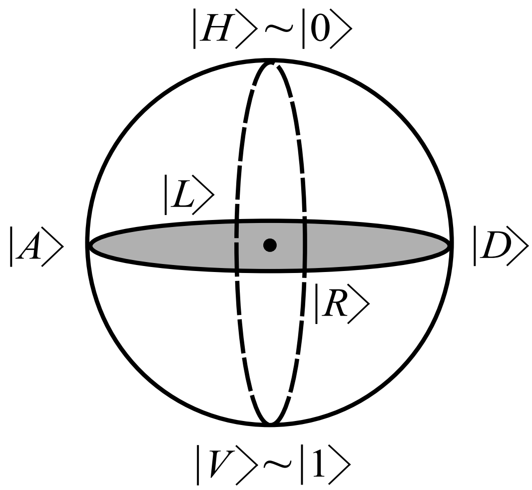

Figure 2.2: Bloch sphere allows easy visualization of polarization states. Polarisation states are labeled as follows: $|H\rangle$ – horizontal, $|V\rangle$ – vertical, $|D\rangle$ – diagonal, $|A\rangle$ – anti-diagonal, $|R\rangle$ – right-hand circular, $|L\rangle$ – left-hand circular.

2.5 Spontaneous parametric down-conversion

One possibility of how to produce entangled photon pairs is the spontaneous parametric down conversion (SPDC) [37]. It is a process which occurs in a non–linear optical media such as for example β–borium borate (BBO) crystal. The incident photon (pump beam) enters the non–linear crystal where it gets annihilated and one pair of photons is created instead. These photons, called signal and idler, are correlated in time. Because the state of the non–linear crystal is unchanged and the laws of energy and momentum conservation apply (see Fig. 2.3), the sum of the signal and idler photon frequencies must be equal to the frequency of the original pumping photon. The same applies to the $\vec{k}$ vectors. This law defines the output vectors of the signal and the idler photon. The condition mentioned above is often called the phase matching. The condition can be fulfilled in an anizotropic media where the refractive

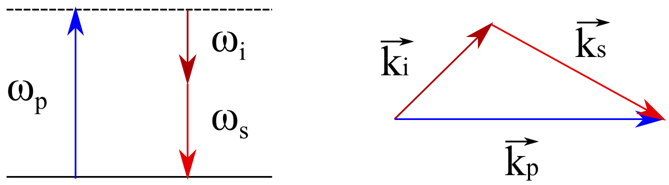

(a) The law of conservation of energy

(b) The law of conservation of momentum

Figure 2.3: Graphical implementation of conservation laws.

index depends on polarization, direction of propagation and frequency.

Let's assume, for simplicity, a negative uniaxial crystal, therefore $n_e < n_o$. Using the polarization of the interacting electromagnetic fields, one can define two types of phase matching. During the Type I process, one photon with extraordinary polarization (e) generates two photons with ordinary polarization (o). On the other hand, in the Type II process one photon with e–polarization generates pair of photons with mutually prependicular e, o–polarizations.

The SPDC process is in general non–collinear, however with suitable geometrical setup the three photons can propagate in the same direction, therefore in special case, the SPDC process can be collinear.

SPDC is stimulated by vacuum fluctuations in signal and idler mode, hence the SPDC process generates photon pairs at random times. Also the conversion efficiency is in currently available media quite low. Only one photon pair out of 10^{12} incident photons is created [38].

2.5.1 Type I

During the non-collinear SPDC process the generated photons can be found on a surface of a cone whose axis is identical with pump beam [39]. The condition on phase matching guarantees that the generated photons with same frequencies are emitted from the crystal on the opposite sides of the cone surface (see Fig. 2.4). The polarization of the created photons is perpendicular to the polarization of the pump beam, therefore, with only one Type I crystal, we can not generate photons with polarization entanglement.

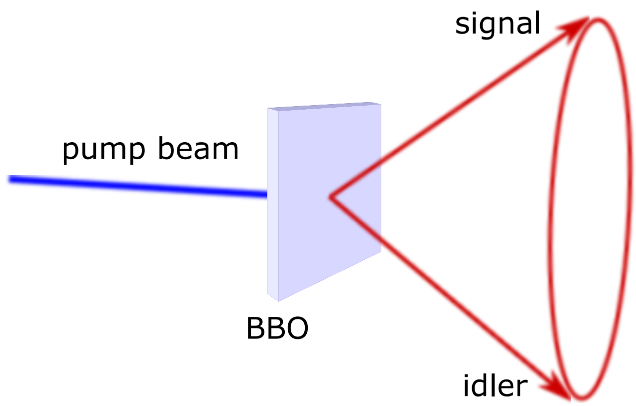

Figure 2.4: The scheme for Type I SPDC process, the generated photons with same frequencies are emitted from the crystal on the opposite sides of the cone surface.

2.5.2 Type II

Type II SPDC process generates photon pairs with mutual prependicular polarizations. The photons are emitted from the crystal into the surfaces of two cones which can intersect in two, one or zero points in dependence on the direction of the main axis of non–linear crystal toward the interface and the direction of the pump beam (see Fig. 2.5) [39]. The generated photons are entangled in polarization only in the intersections of the cones where one can not distinguish single and idler photons apart.

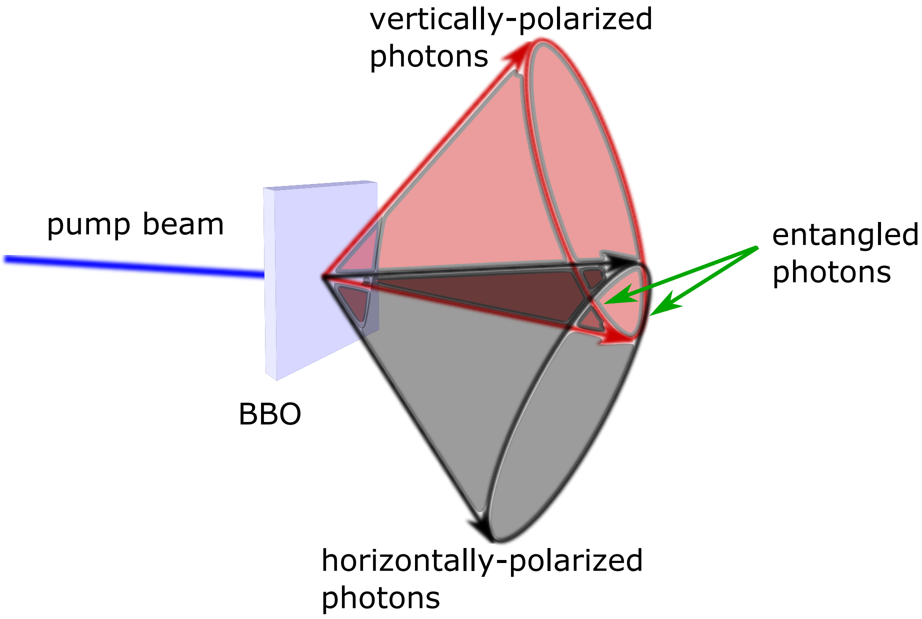

Figure 2.5: The scheme for Type II SPDC process the photons are emitted from the crystal into the surfaces of two cones which can intersect in two, one or zero points. Also the generated photons are entangled in plarization only in the intersections of the cones.

2.5.3 The Kwiat source of entangled photons

Another method allowing to generate photons entangled in polarization is the Kwiat source (also known as crystal cascade) which is made out of two Type I crystals placed in a way that their main planes are mutually orthogonal [39, 40]. The main plane is defined by the direction of the $\vec{k}$ vector and the optical axis. Using vertically polarized pump beam, the SPDC can only occur in the first crystal so the produced cones will contain horizontally polarized photons. Similarly, with horizontally polarized pump beam SPDC will occur only in the second crystal producing identical cones only with vertically polarized photons (see Fig. 2.6). For the pump beam with equal power in both the horizontal and

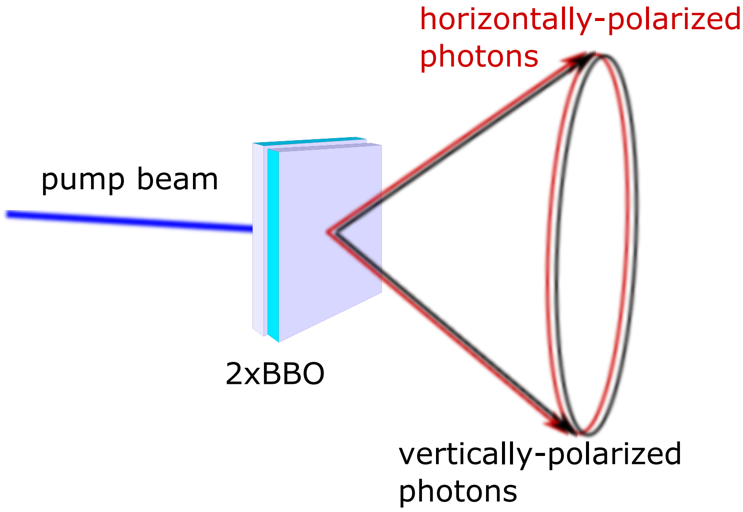

Figure 2.6: The scheme for the Kwiat source of entangled photons.

vertical polarization modes, SPDC can occur in either of the crystals with the same probability. Consequently, the photons will be created in the state $|\psi\rangle = |HH\rangle + e^{i\phi}|VV\rangle$. The ϕ is determined by the phase matching and pump beam state. This way we can relatively easily tune the degree of entanglement. As long as the crystals are thin the trajectories of the generated photons overlap, therefore we can not tell in which crystal the photons originated. This way we can directly prepare photons with polarization entanglement.

2.6 Beam splitter

The beam splitter has an irreplaceable role in quantum optics. It is a key component for quantum gates [41].

Let us denote E_1 and E_2 the amplitudes of electromagnetic fields that enter the beam splitter and E_3 and E_4 amplitudes of fields that exit it. Amplitude E_3 transforms according to $E_3 \rightarrow tE_1 + rE_2$, where t, r are the transmission and reflection coefficients respectively. The coefficients are complex numbers

$t = |t|e^{i\theta}$ and $r = |r|e^{i\phi}$ [42]. Likewise, $E_4 \to tE_2 + rE_1$. The transformation matrix than takes the form of

$$\begin{pmatrix} E_3 \\ E_4 \end{pmatrix} \to \begin{pmatrix} t & r \\ r & t \end{pmatrix} \begin{pmatrix} E_1 \\ E_2 \end{pmatrix}. \tag{2.38}$$

Let us assume that the beam splitter is lossless which is good approximation for most applications. For lossless beam splitter, the transformation matrix $\mathcal{A}$ is unitary. That means that

$$\mathcal{A}^{-1}\mathcal{A} = \mathcal{A}^{\dagger}\mathcal{A} = 1 \Rightarrow \mathcal{A}^{-1} = \mathcal{A}^{\dagger}, \tag{2.39}$$

the equation (2.38) implies that the transformation matrix must satisfy the equation

$$\begin{pmatrix} t & r \\ r & t \end{pmatrix} \begin{pmatrix} t^* & r^* \\ r^* & t^* \end{pmatrix} = \begin{pmatrix} 1 & 0 \\ 0 & 1 \end{pmatrix}, \tag{2.40}$$

which gives the conditions

$$|t|^2 + |r|^2 = 1 \tag{2.41}$$

$$r^*t + rt^* = 0. \tag{2.42}$$

Let us set $\theta = 0$, then Eq. (2.42) simplifies to the form of $2rt\cos\phi = 0$, from which we can easily deduce that $\phi = \pi/2$. For a 50/50 beam splitter the transmission and reflection coefficients are $1/\sqrt{2}$ and the trasformation matrix is in the form of

$$\mathcal{A} = \frac{1}{\sqrt{2}} \begin{pmatrix} 1 & i \\ i & 1 \end{pmatrix}. \tag{2.43}$$

Quantum theory replaces amplitudes by annihilation and creation operators ($\hat{a}$, $\hat{a}^{\dagger}$). It can be shown that Eq. (2.39) holds and the operators are transformed in a identical fashion. Let us denote $\hat{a}_{in}$, $\hat{b}_{in}$ as the input modes and $\hat{a}_{out}$, $\hat{b}_{out}$ as the output modes (see Fig. 2.7). The lossless beam splitter is then described by unitary transformation

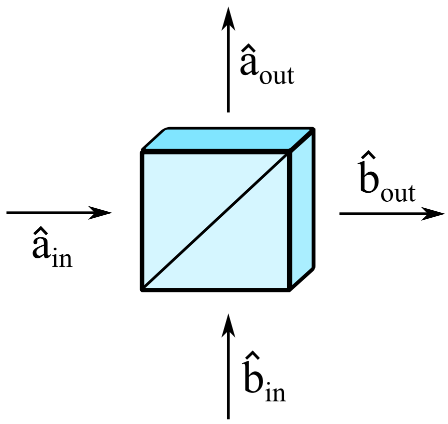

Figure 2.7: The scheme of the beam splitter, that provides the unitary trasformation operation on the input modes.

$$\begin{pmatrix} \hat{a}^{\dagger}_{out} \\ \hat{b}^{\dagger}_{out} \end{pmatrix} = \begin{pmatrix} t & ir \\ ir & t \end{pmatrix} \begin{pmatrix} \hat{a}^{\dagger}_{in} \\ \hat{b}^{\dagger}_{in} \end{pmatrix}. \tag{2.44}$$

3 Theoretical model

Text in chapters 3 and 4 is adopted from V. Trávníček, K. Bartkiewicz, A. Černoch and K. Lemr, "Experimental characterization of photon-number noise in Rarity-Tapster type interferometers," submitted (2017), ArXiv:1704.07590.

Let us denote $|\psi_s\rangle$ the state of signal and idler modes of the SPDC generated photons (Nos. 1 and 2) and $|\alpha\rangle$ the coherent state of the attenuated fundamental laser mode (No. 3). We start with the Hamiltonian for SPDC process in the form of [43]

$$\hat{H}_{\mathrm{SPDC}} = \gamma\alpha_p \hat{a}_1^\dagger \hat{a}_2^\dagger + h.c., \tag{3.1}$$

where $\gamma \ll 1$ is an interaction constant, α_p is a strong pumping amplitude of frequency doubled laser beam and $\hat{a}_1^\dagger$, $\hat{a}_2^\dagger$ are creation operators of the idler and signal photon modes respectively. The corresponding evolution operator is then of the form of

$$\hat{U} = \exp\left(\frac{i}{\hbar}\hat{H}t\right). \tag{3.2}$$

We can aproximate this evolution operator by first three terms of its Taylor expansion

$$\hat{U} \approx 1 + \frac{i\hat{H}t}{\hbar} + \left(\frac{it}{\hbar}\right)^2 \frac{\hat{H}^2}{2}. \tag{3.3}$$

The state of the signal and idler modes is obtained by applying the $\hat{U}$ operator to the initial vacuum state

$$|\psi_s\rangle \propto |00\rangle + \frac{it}{\hbar}\gamma\alpha_p|11\rangle + \frac{(it\gamma\alpha_p)^2}{2\hbar^2}|22\rangle. \tag{3.4}$$

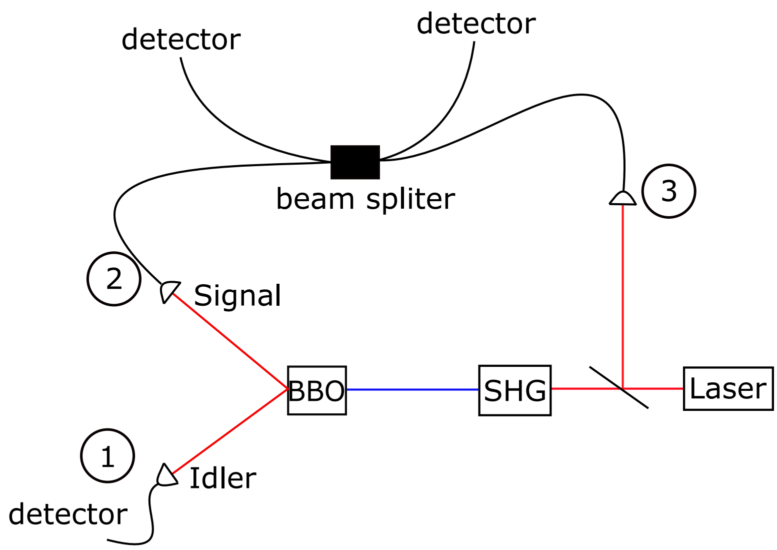

Figure 3.1: Scheme of the experiment, 1 – idler mode, 2 – signal mode, 3 – attenuated fundamental laser mode, SHG – second harmonics generation, Laser – Ti-sapphire fs laser (central wavelength of 826 nm, FWHM of 11 nm), BBO – a β-BaB_2O_4 crystal for SPDC.

Let us introduce a substitution variable

$$\kappa = \frac{it}{\hbar}\gamma\alpha_p, \tag{3.5}$$

so we can express the state $|\psi_s\rangle$ in a compact form

$$|\psi_s\rangle \propto |00\rangle + \kappa|11\rangle + \frac{\kappa^2}{2}|22\rangle. \tag{3.6}$$

The term $|00\rangle$ can be omitted because the first photon works as a herald which means that if it does not get detected the measurment will not succeed. Furthermore, we have to take into account probability of coupling the photons from SPDC into optical fibers. Let us denote t_1 and t_2 the amplitude coupling efficiency of idler and signal modes respectively. The state of the first and second photon then reads

$$|\psi_s\rangle \propto 2\kappa t_1 t_2|11\rangle + 2\kappa t_1\sqrt{1-t_2^2}|10\rangle + \\ + \kappa^2 t_1\sqrt{1-t_1^2}t_2^2|12\rangle + \kappa^2 t_1^2 t_2^2|22\rangle, \tag{3.7}$$

where again we have excluded the terms corresponding to the first mode being in a vacuum state. Moreover, the last term in Eq. (3.7) can be neglected with respect to the third term since in typical experimental setups $t_{1,2} \ll 1$.

Next, we can express the coherent state of attenuated fundamental laser mode in Fock basis and limit the expansion to first four terms

$$|\alpha\rangle \approx |0\rangle + \alpha|1\rangle + \frac{\alpha^2}{\sqrt{2}}|2\rangle + \frac{\alpha^3}{\sqrt{6}}|3\rangle. \tag{3.8}$$

Any filtering or coupling efficiency do not change the nature of the attenuated laser mode which remains in a coherent state with amplitude α already including all possible losses. Thus we do not need to consider its coupling efficiency like in the SPDC modes.

If the source were to be perfect, there should be precisely one photon in each of the three modes. Simultaneous detection of these photons corresponds to genuine coincidences denoted CC_g. In reality, SPDC-based sources yield also higer-photon-number contributions. On the beam splitter, these photons may split leading to three-photon detection even if there were no photons in the attenuated laser mode [see the third term in Eq. (3.7)]. These detections denoted CC_s contribute to added noise. Similar source of noise are higer photon-number contributions from the fundamental laser mode that again can split on the beam splitter resulting in parasitic detections CC_f. Using Eqs. (3.7) and (3.8), we can identify the generation probabilities of the genuine coincidences as well as of the two parasitic contributions

$$CC_g \propto |\kappa|^2|\alpha|^2 t_1^2 t_2^2, \tag{3.9}$$

$$CC_s \propto t_1^2 t_2^4 \frac{|\kappa|^4}{4}, \tag{3.10}$$

$$CC_f \propto |\kappa|^2 t_1^2 \left(\frac{|\alpha|^4}{2} + \frac{|\alpha|^6}{6} \right). \tag{3.11}$$

Note that in Eq. (3.10), we have assumed $1-t_1^2 \approx 1$ and in Eq. (3.11) $1-t_2^2 \approx 1$. These approximation are valid especially when one considers a linear–optical setup fed by the source which strongly diminishes the transmisivity due to technological losses (back–scattering, fiber coupling etc.)

The goal now is to maximize the signal-to-noise ratio defined as

$$\mathrm{SNR} \equiv \frac{CC_g}{CC_s + CC_f} = \frac{12|\alpha|^2 t_2^2}{3|\kappa|^2 t_2^4 + 6|\alpha|^4 + 2|\alpha|^6}. \tag{3.12}$$

In a typical setup as depicted in Fig. 4.1, there are two parameters that can easily be tuned: (i) amplitude of the attenuated fundamental laser mode α and (ii) SPDC pumping amplitude α_p. In subsequent analysis, we investigate the dependency of SNR on these two parameters.

First we look at SNR as function of α, which translates to the observed ratio R between coincidence rates CC_f and CC_s

$$R \equiv \frac{CC_f}{CC_s} = \frac{2|\alpha|^4}{|\kappa|^2 t_2^4} + \frac{2|\alpha|^6}{3|\kappa|^2 t_2^4} \approx \frac{2|\alpha|^4}{|\kappa|^2 t_2^4}. \tag{3.13}$$

We have omitted the second expansion term from CC_f because for typical levels of attenuation to single-photon level $|\alpha| \ll 1$. The signal-to-noise ratio can now be expressed as function of the parameter R

$$\mathrm{SNR} \approx \frac{2\sqrt{2R}}{|\kappa|(R+1)}. \tag{3.14}$$

One can now find optimal value of R by searching for maximum of this function. When $|\alpha| \ll 1$ holds, the optimal value of R is 1. For larger values of $|\alpha|$ the optimal R shifts to slightly lower values because the approximation in Eq. (3.13) does not longer apply. In an experiment, one should thus seek to balance the false coincidence rates from SPDC and from attenuated fundamental mode.

In the subsequent analysis, we assume that $|\alpha| \ll 1$ holds and fix the parameter R at its optimal value of 1. The Eq. (3.14) then simplifies into the form

$$\mathrm{SNR} = \frac{2\sqrt{2}}{|\kappa|}, \tag{3.15}$$

which can, with the help of Eqs. (3.9) and (3.13), be expressed in terms of the genuine coincidence rate CC_g

$$\mathrm{SNR} \propto \sqrt[3]{\frac{16t_1^2t_2^4}{CC_g}}. \tag{3.16}$$

One can now make two important conclusions towards the performance of the interferometer. Firstly, the SNR can only be increased by decreasing the value of $|\kappa|$ which means by lowering the SPDC pumping strength $|\alpha_P|$. Secondly, the obtained coincidence rate depends on the coupling efficiency of the signal and idler SPDC modes. Especially, it scales with the fourth power of the amplitude transmissvity of the signal mode (or second power of intensity transmissivity). For any given pumping strength, one can improve the overall coincidence rate by improving the coupling efficiencies. The SNR, however, can not be improved by this adjustment.

4 Experiment

We have subjected our model and the resulting conclusions to an experimental test. Our experimental setup is depicted in Fig. 4.1. The attenuated fundamental laser mode (mode No. 3) is obtained by splitting a small portion from the femtosecond pumping laser beam (Coherent Mira at 826 nm). It then passes through a neutral density filter (NDF3) and 3nm-wide interference filter (IF3) before been coupled into single-mode fiber.

The main laser beam enters second harmonics generation unit (SHG), where its wavelength becomes 413 nm. The beam then passes through a neutral density filter (NDF1) and enters a Type I cut BBO crystal (0,64 mm thick) which due to SPDC generates idler and signal photons (Nos. 1 and 2) respectively. The photons in signal mode then pass through a 3nm-wide interference filter (IF2). The photons in idler mode pass through a 10nm-wide interference filter (IF1). The two SPDC modes are then coupled into single-mode fibers, idler mode is directly lead to a single-photon detector unlike the modes 2 and 3 that are mixed in a 50:50 fiber coupler before being detected. The avalanche photodiode detectors with suitable electronics record three-fold coincidence detections. Coincidence detection window was set to 5 ns, less than the laser repetition period of approximately 12,5 ns. We set the temporal displacement between photons 2 and 3, so they do not overlap in the fiber coupler. Thus we prevent the effect of two-photon interference.

In our experiment, we performed all the testing measurements in three

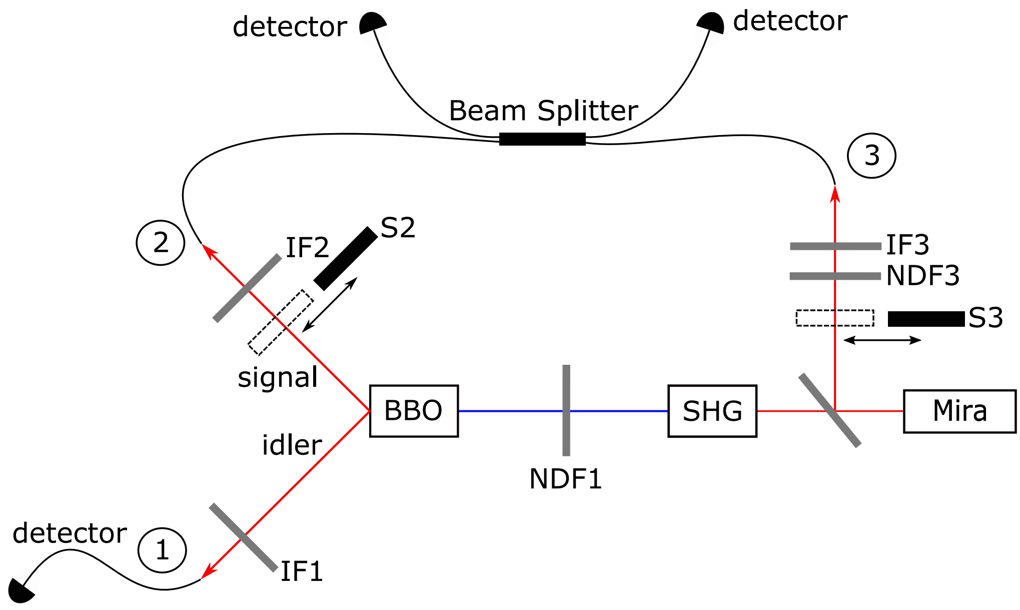

Figure 4.1: Setup of the experiment, 1 – idler mode, 2 – signal mode, 3 – attenuated fundamental laser mode, IF(1-3) – interference filters (3 nm in FWHM), NDF(1,3) – neutral density filter, S(2,3) – shutters, SHG – second harmonics generation, Mira – Ti-sapphire fs laser (central wavelength of 826 nm, FWHM of 11 nm), BBO – a β-BaB_2O_4 crystal for SPDC.

steps: (i) with the shutters S2 and S3 open we detect all three-fold coincidences CC_a which include CC_g and parasitic contributions from signal and attenuated fundamental laser mode CC_s and CC_f

$$CC_a = CC_g + CC_f + CC_s. \tag{4.1}$$

(ii) then we close shutter S3 and obtain three-fold coincedences only if there is more than one photon in signal mode, thus we measure parasitic coincidence rate CC_s. (iii) finally we close shutter S2, open S3 and therefore obtain three-fold coincedences only if there is more than one photon in attenuated fundamental laser mode – parasitic coincidence rate CC_f. Note that CC_g is obtained from Eq. (4.1) simply by subtracting CC_f and CC_s from CC_a. Each step took about 100 s and the entire three-step procedure was reapeted multiple times, thus we have avioded a bias caused by long-term laser power fluctuations.

First, we have experientially verified the dependence of SNR on α, hence as a function of R [see Eq. (3.14)]. The experiment consisted of measuring the coincidence rates for various values of R using the above-mentioned three steps. The parameter R was changed by modifying transmissivity of NDF3. Experimentally obtained values are summarized in Tab. 4.1 and visualized in Fig. 4.2 together with the theoretical fits based on Eq. (3.14). The dashed line shows a fit in which we limited the expansion in Eq. (3.8) to the first three terms, however it turns out that the model is not accurate enough for $R \to 10$ (see Fig. 4.2). With growing contribution of parasitic coincidences from the attenuated fundamental laser mode CC_f, and thus also growing ratio R, higher terms in Eq. (3.8) can no longer be neglected and the approximation in Eq. (3.13) does no longer hold. The solid line which represents a model where we used the first four terms of the expansion, is accurate enough throughout the entire measured range of R. We went a step further and expended our model (represented in Fig. 4.2 by dash-dot line) to include the first five terms of the expansion. There is a slight but unsubstantial improvement to the previous case and thus we find the four-term expansion to be the optimum compromise between accuracy and complexity. To simplify the following experiments, we have set the attenuated laser beam power so that the approximation in Eq. (3.13) holds. This means setting R $\in$ [0.2;1] which also coincides with the SNR maximum.

As the next test, we have measured the dependence of SNR on the pumping amplitude α_p, which also translates into the dependence of SNR on the genuine coincidence rate CC_g [see Eqs. (3.15) and (3.16)]. We maintained the ratio R

SNR [dB]	parameter R
-6.222 ± 0.740	0.013 ± 0.004
-4.440 ± 0.432	0.030 ± 0.004
-3.010 ± 0.440	0.040 ± 0.006
-1.105 ± 0.388	0.080 ± 0.008
-0.530 ± 0.442	0.340 ± 0.021
-0.086 ± 0.392	1.130 ± 0.052
-2.201 ± 0.241	1.510 ± 0.057
-3.502 ± 0.667	3.290 ± 0.290
-6.434 ± 0.727	7.180 ± 0.680

Table 4.1: Experimentaly observed data and their respective errors when investigating the dependence of SNR on the parameter R

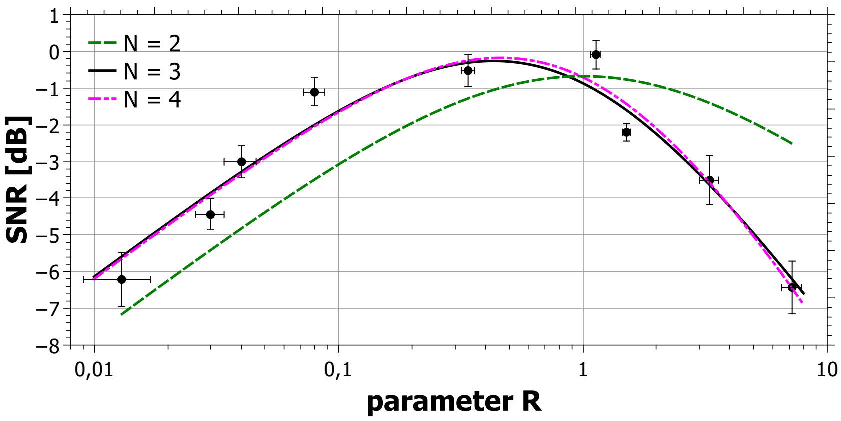

Figure 4.2: Dependence of SNR on parameter R. Points visualize experimentally observed results. Lines correspond to various levels of expension in Eq. (3.8): to 2 (green dashed line), 3 (black solid line), 4 (magneta dashed-dot line) terms.

SNR [dB]	**CC**$_g$ **per** $100\,\mathrm{s}$	$P_p \propto |\alpha_p|^2$ **[mW]**
9.91 ± 1.274	2.91 ± 0.111	13 ± 2
7.50 ± 0.787	7.23 ± 0.217	25 ± 2
6.23 ± 0.714	19.88 ± 0.613	50 ± 2
5.17 ± 0.559	51.59 ± 1.384	104 ± 3
3.33 ± 0.577	135.28 ± 4.392	190 ± 3

Table 4.2: Experimentally observed data and their respective errors when investigating the dependence of SNR on the CC_g and CC_g on the α_p.

close to its optimum discovered in previous test ($R \approx 0.35 \pm 0.04$) and were changing α_p by changing transmissivity of NDF1. So for every measured value of SNR, we have adjusted both the NDF1 (influencing α_p) and NDF3 (to maintain constant R). The measurement procedure was also realised in the previously mentioned three acquisition steps. Experimentally obtained values are summarized in Tab. 4.2 and visualized in Fig. 4.3 together with a theoretical fit based on Eq. (3.15). The Fiq. 4.3 proves that our four-term model matches well the experimental data. We have also investigated dependence of CC_g on pumping power P_p which is proportional to pumping amplitude $|\alpha_p|^2$.

The final two tests of our model involved verifying the dependence of genuine coincidence rate CC_g on the coupling efficiencies (i) t_1 and (ii) t_2 as predicted in Eq. (3.16). During each of the two tests, the parameter R and the pumping power were kept constant resulting in constant SNR. During the first test the value of SNR was $(4{,}7 \pm 1{,}6)\,\mathrm{dB}$. In the second test the SNR was $(5{,}0 \pm 1{,}3)\,\mathrm{dB}$. In order to test the dependence on idler and signal mode transmissivities t_1 and t_2, we have acquired the coincidences in the usual three steps for various levels of attenuation by closing a diaphragm on the idler and

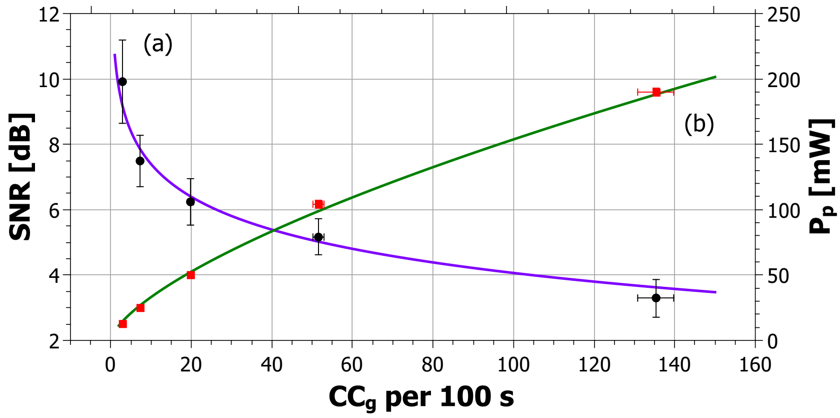

Figure 4.3: (a) Dependence of SNR on genuine coincidence rate CC_g. Points visualize experimentally observed results, the solid violet line depicts fitted experimental data with theoretical dependence based on Eq. (3.15). (b) Dependence of CC_g on P_p. The solid green line depicts fitted experimental data with theoretical dependence based on Eq. (3.9)

signal mode fiber couplers respectively. When the signal mode attenuation was set, the NDF3 in the attenuated fundamental laser mode was readjusted to maintain a constant R. This was not necessary when closing the idler mode diaphragm. For better readability of our results, we introduce the idler and signal mode intensity attenuation factors A_1 and A_2 so that the modes' transmissivities become $t_j^2 \to t_j^2/A_j$ for $j = 1, 2$. Experimentally observed values are summarized in Tab. 4.3 and visualized in Fig. 4.4. Fig. 4.4 demonstrates that with constant SNR CC_g dependents on modes' transmissivities t_1^2 and t_2^2 as functions $\frac{1}{x}$ and $\frac{1}{x^2}$ respectively as predicted in Eq.(3.16).

idler attenuation (t_1)		signal attenuation (t_2)	
$\mathbf{A}_1$	$\mathbf{CC}_g$ per 100 s	$\mathbf{A}_2$	$\mathbf{CC}_g$ per 100 s
1	41.2 ± 3.2	1	44.8 ± 2.5
1.4	27.2 ± 1.7	1.3	22.2 ± 1.5
2	19.0 ± 1.7	1.9	10.0 ± 1
2.7	14.3 ± 1.8	2.8	6.2 ± 1
4	10.0 ± 1.7	3.8	2.3 ± 0.3

Table 4.3: Experimentally observed data and their respective errors when investigating the dependence of CC_g on the attenuation factors A_1 and A_2.

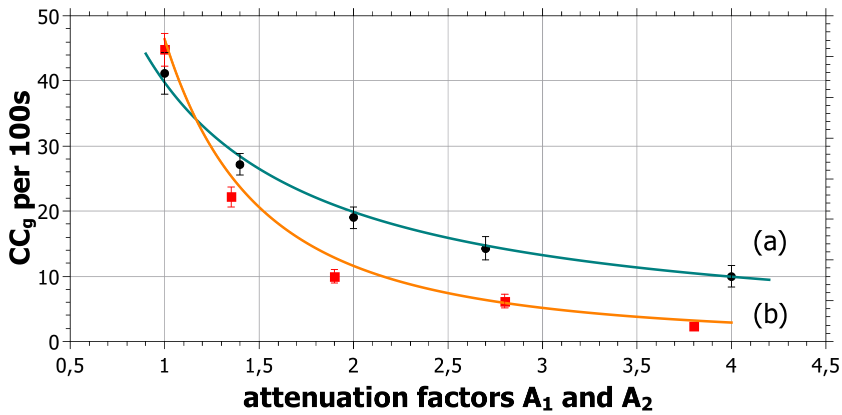

Figure 4.4: (a) Dependence of CC_g on attenuation factor A_1. Points visualize experimentally observed results, the solid blue–green line depicts fitted experimental data with theoretical fit based on Eq. (3.16). (b) Dependence of CC_g on attenuation factor A_2. The solid orange line depicts fitted experimental data with theoretical dependence based on Eq. (3.16).

4.1 Impact of the noise on teleportation fidelity

We now investigate the impact of the above analyzed noise on quantum teleportation. Since quantum teleportation is a key ingredient in many quantum information protocols, it is essential to asses the influence of inherent noise of various photon sources on its performance. In quantum circuits, including teleporation, one often uses fidelity as a measure of the circuits quality. Assuming a pure input qubit state $|\psi\rangle_{in}$ and the resulting teleported state $\hat{\rho}_{out}$, fidelity can be calculated using the formula

$$F = |\langle\psi_{in}|\hat{\rho}|\psi_{in}\rangle|. \tag{4.2}$$

Note that when teleportation is replaced by classical "measure and recreate" protocol, the fidelity can not exceed its classical limit of $\frac{2}{3}$ [44]. Even though it is impossible to reach perfect fidelity $F = 1$ in realistic conditions, one still targets to maximize its value.

In our analysis we have calculated the dependence of average fidelity $\langle F\rangle$ on the signal-to-noise ratio (SNR). If we fix the parameter R to its optimum value ($R \approx 0.35$) the fidelity $\langle F\rangle$ is than a function that depends on CC_g and only one of the CC_s or CC_f since these two are bound by fixed parameter R. As a result the fidelity is a function of SNR. We have calculated the average fidelity using the formula

$$\langle F\rangle = \frac{P_{CC_g}F_g + P_{CC_s}F_s + P_{CC_f}F_f}{P_{CC_g} + P_{CC_s} + P_{CC_s}}, \tag{4.3}$$

where

$$P_{CC_g} = \frac{CC_g}{4f}, P_{CC_s} = \frac{CC_s}{4f}, P_{CC_f} = \frac{CC_f}{4f}, \tag{4.4}$$

are the probabilities of the coincidence events. f stands for the repetition rate of the pumping laser and F_g, F_s, F_f are the teleportation fidelities if the coincidence CC_g, CC_s or CC_f occur respectively. The value of teleportation fidelity $F_g = 1$ because from the definition there is one photon in each mode so the teleportation succeeds perfectly, at least in principle. On the other hand, the teleportation fidelities F_s and F_f have values of $\frac{1}{2}$. First one because the two

fidelity F	fidelity uncertainty interval	SNR [dB]
0.96	$\langle 0.93, 0.98\rangle$	9.91 ± 1.27
0.94	$\langle 0.90, 0.96\rangle$	7.50 ± 0.79
0.92	$\langle 0.86, 0.95\rangle$	6.23 ± 0.71
0.89	$\langle 0.85, 0.91\rangle$	5.17 ± 0.56
0.85	$\langle 0.83, 0.86\rangle$	3.29 ± 0.58

Table 4.4: Calculated data and their respective errors when investigating the dependence of average fidelity F on the SNR.

photons in signal mode are randomly projected onto Bell states uncorrelated with the teleported photon which is missing. The later because the two photons in attenuated laser mode are not correlated with the idler mode which is thus a mixed state.

Calculated values are summarized in Tab. 4.4 and visualized in Fig. 4.5. We observe that the average fidelity drops only slightly with decreasing SNR, so the average fidelity is above 80% for SNR around 3 dB. However this does not take into account other experimental imperfections (such as two–photon overlap, polarization adjustments etc.) that combining with photon-number noise can lead to such a low fidelity that the protocol fails. The fidelity uncertainty intervals were calculated using a Monte–Carlo simulation based on poisson distribution of detected coincidences.

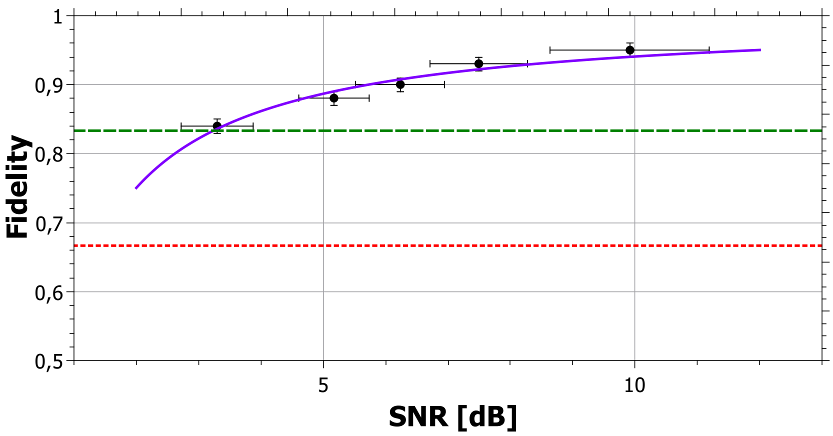

Figure 4.5: Dependence of average fidelity $\langle F \rangle$ on SNR. Points visualize calculated results from experimentally observed SNRs. The solid violet line corresponds to our theoretical model, the dotted red line is the classical protocol limit ($F = 2/3$) [44] and the dashed green line indicates the secure teleportation, i.e., $F = 5/6$ cloning threshold see [45].

5 Hong-Ou-Mandel interference

One example where we can make use of our model is the Hong–Ou–Mandel interference [41] which is a vital component for quantum information processing with light. In this phenomenon, two photons are mixed on a beam splitter and if they are indistinguishable in all degrees of freedom, they interfere leaving the beam splitter together by one output mode. In the previous experiments, we intentionally made sure that the photons from signal and fundamental mode will not arrive to the beam splitter at the same time because the interference offect will obstruct coincidence measurments. In this measurment however, we wanted them to overlap resulting in dip in coincidence counts.

First, we had to find the position overlap, that was done by lengthening the distance of the fundamental mode coupler and measuring the number of three-fold coincidences as a function of the coupler's position. When the coupler position matches the photons overlap on the beam splitter, the number of coincidences drops (HOM dip).

Fig. 5.1 shows a naive approach in which we did not optimize anything like if we were not aware of our model for photon–number noise. The pump power was at 100 % (190 mW), the false coincidences constitute 44 % of all the three–fold detections. We used a 10 nm interference filter in the idler mode. Visibility as a metric of quality is defined as

$$V = \frac{M - m}{M + m}, \tag{5.1}$$

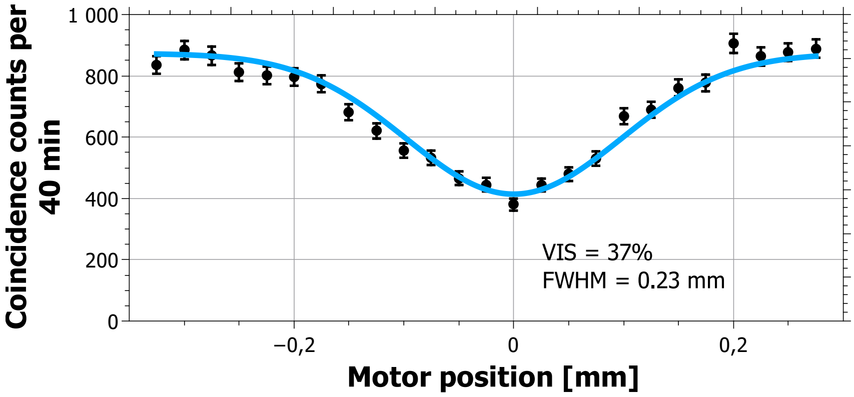

Figure 5.1: Dependence of coincidence counts on motor position. Points visualize experimentally observed results, the solid blue line depicts fitted experimental data with Gaussian function. VIS stands for visibility, FWHM is Full Width at Half Maximum.

where M is the maximum number of coincidences and in the opposite m is defined as the minimum number of coincidences. In this case the visibility was a mere 37 %.

In the next measurment, we set the ratio of fundamental–mode and SPDC–mode based false coincidences R to its optimum value. The pump power was again at 100 % (190 mW), the false coincidences droped to 28 %. In the Fig.5.2 we can see better results as the visibility reaches 45 %.

The model tells us that for higher visibility we should lower the pump power while maintaning R on its optimum. The power was thus set to 33 % (63 mW), the false coincidences dropped to 17 %. Also we used 3 nm interference filter in the idler mode. This way we can further reduce false coincidences from fundamental mode. The Fig.5.3 shows the results with visibility of 72 %.

In the Fig.5.4 yet another measurment is depicted. The pump power was at 25 % (48 mW) and the false coincidences at 12 % resulting in highest observed

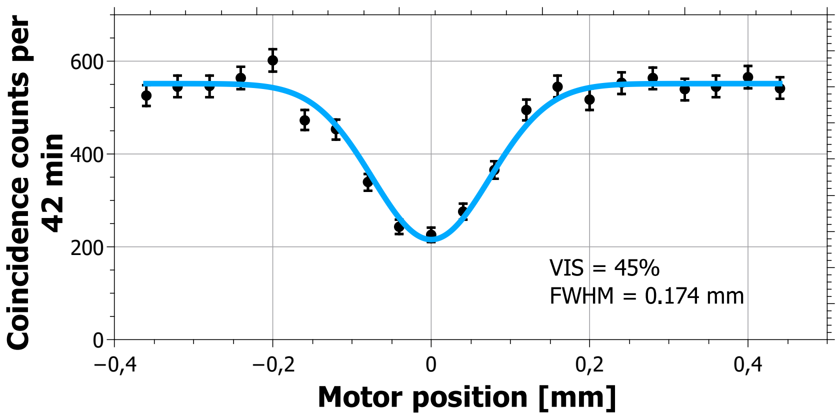

Figure 5.2: Dependence of coincidence counts on motor position. Points visualize experimentally observed results, the solid blue line depicts fitted experimental data with Gaussian function. VIS stands for visibility, FWHM is Full Width at Half Maximum.

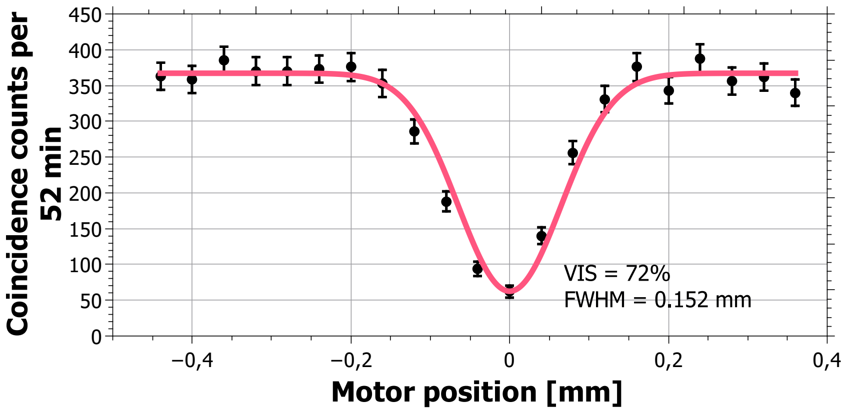

Figure 5.3: Dependence of coincidence counts on motor position. Points visualize experimentally observed results, the solid pink line depicts fitted experimental data with Gaussian function. VIS stands for visibility, FWHM is Full Width at Half Maximum.

visibility of 74 %. There is also a downside, by lowering the pump power the three–fold coincidences are scarce which is a problem for parctical usage. Note that while in the first case, we observed about 22 coincidences per minute, in the case of highest visibility there was only abou 4.5 coincidences per minute

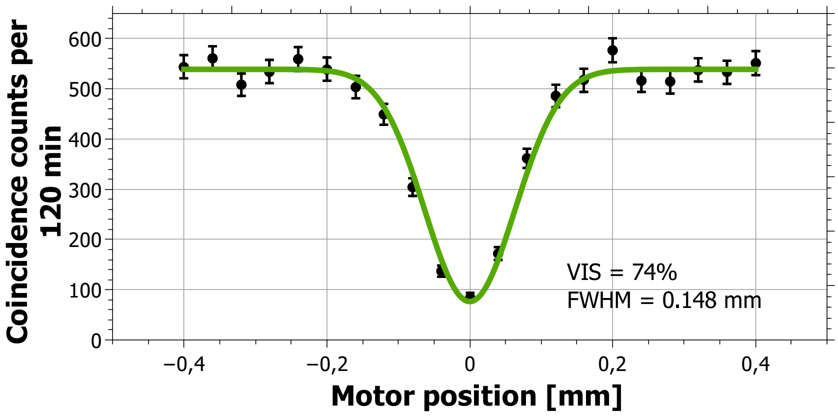

Figure 5.4: Dependence of coincidence counts on motor position. Points visualize experimentally observed results, the solid green line depicts fitted experimental data with Gaussian function. VIS stands for visibility, FWHM is Full Width at Half Maximum.

6 Conclusions

In conclusion, we have shown that our model fits the experimental data very well. We have demonstrated the role of the ratio R between the SPDC-based and attenuated fundamental-based false coincidences. We have also confirmed its optimal value being close to 1 depending on the pumping strength. In the next step, we have verified that SNR (when optimal R) can only be increased by decreasing the SPDC pumping strength. Our data fits well both the SNR as a function of genuine coincidence rate, and also the predicted coincidence rate as a function of pumping strength. Finally, we have successfully tested the genuine coincidence rates as functions of coupling efficiencies while maintaining constant SNR. Our model and the obtained conclusions drawn from it can be useful for experimentalist when constructing a similar three-photon source and using it for teleportation-like protocols. With respect to that, we have made a prediction of the impact of this noise to teleportation fidelity. While fidelity drops smoothly with decreasing SNR, in conjunction with other experimental imperfections it may fall below the classical threshold. The results of the Hong–Ou–Mandel interference prove that our model works properly and can significantly improve the set up for QIP measurements.

Bibliography

[1] M. Planck, *"On the theory of thermal radiation,"* Annalen der Physik **4**, 553–563 (1901).

[2] A. Einstein, *"Concerning an Heuristic Point of View Toward the Emission and Transformation of Light,"* Annalen der Physik **17**, 132 (1905)

[3] L. Skála, Úvod do kvantové mechaniky, Karolinum, Praha (2011), ISBN: 978-80-246-2022-0.

[4] L. Grover, *"A fast quantum mechanical algorithm for database search,"* in: Proceedings of the twenty-eighth annual ACM symposium on Theory of computing, ACM, 212–219 (1996).

[5] P. W. Shor, *"Polynomial-Time Algorithms for Prime Factorization and Discrete Logarithms on a Quantum Computer,"* SIAM J. Sci. Statist. Comput. 26, 1484 (1997).

[6] C. Benett and G. Brassard, *"Quantum Cryptography: Public key distribution and coin tossing,"* in: IEEE International Conference on Computers, Systems, and Signal Processing, Bangalore, 175 (1994).

[7] A. K. Ekert, *"Quantum cryptography based on Bell's theorem,"* Phys. Rev. Lett. 67, 661–663 (1991).

[8] G. Alber, T. Beth, M. Horodecki, P. Horodecki, R. Horodecki, M. Rötteler, H. Weinfurter, R. Werner, and A. Zeilinger, Quantum Information, Springer, Berlin, 2001, ISBN: 978-3-540-41666-1.

[9] M. Nielsen and I. Chuang, Quantum Computation and Quantum Information, Cambridge: Cambridge University Press, 2002, ISBN: 0-521-63235- 8.

[10] D. Bowmeester, A. Ekert, and A. Zeilinger, The Physics of Quantum Information, Springer, Berlin, 2000, ISBN: 978-3-642-08607-6.

[11] P. Kok, W. J. Munro, K. Nemoto, T. C. Ralph, J. P. Dowling, and G. J. Milburn, *"Linear optical quantum computing with photonic qubits,"* Rev. Mod. Phys. **79**, 135 (2007).

[12] X.-S., Ma, T. Herbst, T. Sheidl, *"Quantum teleportation over 143 kilometres using active feed-forward,"* Nature **489**(7415) (2012)

[13] Q.-C. Sun, Y.-L. Mao, S.-J. Chen, W. Zhang, *"Quantum teleportation with independent sources and prior entanglement distribution over a network,"* Nature Photonics **10**, 671–675 (2016).

[14] C. Benett, G. Brassard, C. Crépeau, R. Jozsa, A. Peres, and W. Wootters, *"Teleporting an Unknown Quantum State via Dual Classical and Einstein- Podolsky-Rosen Channels,"* Phys. Rev. Lett. **70**, 1895 (1993).

[15] D. Bouwmeester, J. Pan, K. Mattle, M. Eibl, H.Weinfurter, and A. Zeilinger, *"Experimental quantum teleportation,"* Nature (London) **390**, 575 (1997).

[16] X.-s. Ma, S. Zotter, J. Kofler, R. Ursin, T. Jennewein, Č. Brukner and A. Zeilinger, *"Experimental delayed-choice entanglement swapping,"* Nature Physics **8**, 479–484 (2012).

[17] W. Tittel, J. Brendel, B. Gisin, T. Herzog, H. Zbinden, and N. Gisin, *"Experimental demonstration of quantum correlations over more than 10 km,"* Phys. Rev. A **57**, 3229 (1998).

[18] D. Gottesman, I. L. Chuang, *"Demonstrating the viability of universal quantum computation using teleportation and single-qubit operations,"* Nature **402**, 390-393 (1999).

[19] J. G. Rarity, P. R. Tapster and R. Loudon, *"Non-classical interference between independent sources,"* Journal of Optics B: Quantum and Semi-classical Optics **7** 1464 (2005).

[20] B. Lounis and M. Orrit, *"Single-photon sources,"* Reports on Progress in Physics **68** 0034-4885-R04 (2005).

[21] S. Scheel, *"Single-photon sources–an introduction,"* Journal of Modern Optics **56**(2-3) (2009).

[22] C. Vitelli, N. Spagnolo, L. Aparo, F. Sciarrino, E. Santamato, and L. Marrucci, *"Joining the quantum state of two photons into one,"* Nat. Photon. **7**, 521–526 (2013).

[23] K. Lemr, A.Černoch, J. Soubusta, K. Kieling, J. Eisert, and M. Dušek, *"Experimental implementation of the optimal linear-optical controlled phase gate,"* Phys. Rev. Lett. **106**, 13602 (2011).

[24] K. Lemr, K. Bartkiewicz, A. Černoch, M. Dušek, and J. Soubusta, *"Experimental Implementation of Optimal Linear-Optical Controlled-Unitary Gates,"* Phys. Rev. Lett. **106**, 153602 (2015).

[25] X.-L. Wang, L.-K. Chen, W. Li, *"Experimental Ten-Photon Entanglement,"* Phys. Rev. Lett. **117**, 210502 (2016).

[26] G. Brassard, N. Lütkenhaus, T. Mor, and B. C. Sanders, *"Limitations on Practical Quantum Cryptography,"* Phys. Rev. Lett. **85**, 1330 (2000).

[27] Y. Zhao, B. Qi, X. Ma, H.-K. Lo, and L. Qian, *"Experimental Quantum Key Distribution with Decoy States,"* Phys. Rev. Lett. **96**, 070502 (2006).

[28] J. Peřina, Quantum Statistics of Linear and Nonlinear Optical Phenomena, Springer, Netherlands, (1991), ISBN 9789401124003.

[29] L. Mandel and E. Wolf, Optical coherence and quantum optics, Cambridge University Press, New York (1995), ISBN 0521417112.

[30] M. Vrbová, Kvantová teorie koherence, České Vysoké Učení Technické v Praze, Praha (1997).

[31] C. E. Shannon, *"A mathematical theory of Communication,"* The Bell system technical journal **27**, 379–423 (1948).

[32] M. Nielsen and I. Chuang, Quantum Computation and Quantum Information, Cambridge University Press, Cambridge (2002).

[33] B. Schumacher, *"Quantum coding,"*. Physical Review A. **51** (4) (1995)

[34] S. Gasparoni, J. Pan, P. Walther, T. Rudolph, and A. Zeilinger, *"Realization of a Photonic Controlled-NOT Gate Sufficient for Quantum Computation,"* Phys. Rev. Lett. **93**, 020504 (2004).

[35] M. Mohseni, A. M. Steinberg, and J. A. Bergou, *"Optical realization of optimal unambiguous discrimination for pure and mixed quantum states,"* Phys. Rev. Lett. **93**, 200403 (2004).

[36] L. Bartůšková, A. Černoch, R. Filip, J. Fiurášek, J. Soubusta, and M. Dušek, *"Optical implementation of the encoding of two qubits to a single qutrit,"* Phys. Rev. A **74** (2), 022325 (2006).

[37] B. E. Saleh, M. C. Teich, Fundamentals of Photonics, 2nd ed. Wiley (2007).

[38] A. Ling, A. Lamas-Linares, Ch. Kurtsiefer, *"Absolute emission rates of spontaneous parametric down-conversion into single transverse Gaussian modes,"* Physical Review A. **77** (4) (2008).

[39] E. Halenková, A. Černoch and J. Soubusta, Spontánní sestupná frekvenční parametrická konverze a zdroj fotonových párů podle návrhu P.G. Kwiata, Univerzita Palackého v Olomouci, Olomouc (2012), ISBN 978-80-244-3111-6.

[40] P. G. Kwiat, E. Waks, A. G. White, I. Appelbaum, and P. H. Eberhard, *"Ultrabright Source of Polarization-Entangled Photons,"* Phys. Rev. A **60**, R773 (1999).

[41] C. Hong, Z. Ou, and L. Mandel, *"Measerement of Subpicosecond Time Intervals between Two Photons by Interference,"* Phys. Rev. Lett. **59**, 2044 (1987).

[42] R. Loudon, The quantum theory of light, third edition, Oxford University Press, New York (2000).

[43] M. H. Rubin, D. N. Klyshko, Y. H. Shih, A. V. Sergienko, *"Theory of two-photon entanglement in type-II optical parametric down-conversion,"* Phys. Rev. A **50**, 5122 (1994).

[44] S. Popescu, *"Bell's inequalities versus teleportation: What is nonlocality?,"* Phys. Rev. Lett. **72**, 797 (1994).

[45] K. Özdemir, K. Bartkiewicz, Y.-X. Liu, A. Miranowicz, *"Teleportation of qubit states through dissipative channels: Conditions for surpassing the no-cloning limit,"* Phys. Rev. A **76**, 042325 (2007).

7 Appendix

Faculty
of Science

Confirmation of contribution

As the supervisor and corresponding author of Vojtěch Trávníček's publication

- V. Trávníček, K. Bartkiewicz, A. Černoch, and K. Lemr, *"Experimental characterization of photon-number noise in Rarity-Tapster type interferometers,"* submitted (2017), preprint: arXiv:1704.07590

I hereby certify that Vojtěch Trávníček significantly contributed to the scientific investigation presented in this publication as well as to writing of the manuscript. The extracts of the publication directly quoted in his thesis were predominantly written by him.

Olomouc, 26th April 2017

Karel Lemr

....

doc. Mgr. Karel Lemr, Ph.D.
Joint Laboratory of Optics

Experimental characterization of photon-number noise in Rarity-Tapster type interferometers

Vojtěch Trávníček,[1,*] Karol Bartkiewicz,[2,1,†] Antonín Černoch,[1,‡] and Karel Lemr[1,§]

[1] *RCPTM, Joint Laboratory of Optics of Palacký University and Institute of Physics of Czech Academy of Sciences, 17. listopadu 12, 771 46 Olomouc, Czech Republic*

[2] *Faculty of Physics, Adam Mickiewicz University, PL-61-614 Poznań, Poland*

(Dated: April 26, 2017)

In this paper, we develop a simple model describing inherent photon-number noise in Rarity-Tapster type interferometers. This noise is caused by generating photon pairs in the process of spontaneous parametric down-conversion and adding a third photon by attenuating fundamental laser mode to single-photon level. We experimentally verify our model and present resulting signal to noise ratios as well as obtained three-photon generation rates as functions of various setup parameters. Subsequently we evaluate impact of this particular source of noise on quantum teleportation which is a key quantum information protocol using this interferometric configuration.

I. INTRODUCTION

Quantum information processing (QIP) is a modern and perspective reaserch discipline of information science [1–3]. One of the platforms suitable for QIP are discrete photons manipulated using linear optics [4]. This platform is particularly promising for quantum communications, because of fast and relatively noiseless propagation of individual photons through open space or in fibers [5, 6].

Quantum teleportation [7, 8] is a key ingredient for many quantum information protocols such as entanglement swapping [9], quantum relays [10] or teleportation-based quantum computing [11]. On the platform of linear optics, quantum teleportation is usually achieved in the so-called Rarity-Tapster interferometer [12] (shown in Fig. 1). In this interferometer, one photon from an entangled pair gets overlapped on a balanced beam splitter with an independent photon [4]. The output ports of the beam splitter are then subjected to suitable Bell-state projection. Mulitphoton inteferometers have also a number of potential applications that go beyond quantum teleportation (for a review see Ref. [13]). For example, they can be also used for engineering cluster states [14].

Single–photon sources used in experimental quantum information processing today are however imperfect and the number of photons generated per pulse is random, given by the state's photopulse statistics (e.g. Bose-Einstein, Poisson). While vacuum states can be filtered out by suitable post-selection, higher photon-number contributions can not always be recognized [15, 16].

In 1988, Ou and Mandel predicted that visibility of two-photon bunching with classical beams is limited to 50% due to their photon-number statistics [17]. This research was further generalized to interaction between classical beam and ideal single-photon source [12]. Subsequently, researchers have managed to considerably increase visibility in Rarity-Tapster interferometers by optimizing spectral properties of interacting beams [18–20]. Independently, several research groups have investigated two-photon bunching between two heralded single-photon sources [21–23].

In this paper, we present a simple and practical model describing inherent photon-number noise in Rarity-Tapster type interferometers based on sources using spontaneous parametric down conversion (SPDC) and attenuated coherent state. These are currently predominant photon sources in experimental linear-optical QIP [5, 24–29]. We have experimentally tested validity of our model and established both theoretical and experimental relations between photon-number noise and various setup parameters. Our goal was to investigate the effect of photon–number noise originating directly in photon sources. To our best knowledge no article providing such analysis has yet been published. The influence of transmission noise on the fidelity and security of quantum teleportation of qubits was analyzed in Ref. [30]. Photon-number noise does not originate from experimental imperfections but is rather an intrinsic property of various photon sources (having their photon-number statistics). This fact even further stresses out the importance of this investigation.

The paper is organized as follows: In Sec. II we develop a theoretical model describing dependency of signal–to–noise ratio on the main parameters of the experimental setup. In Sec. III we present experimnetal data verifing our model. In Sec. IV we investigate the impact of the photon–number noise on teleporation fidelity. We conclude in Sec. V.

II. THEORETICAL MODEL

Here, we assume that the pairs of photons are generated in the process of degenerate parametric down conversion. The generated optical fields are not strictly

*Electronic address: vojtech.travnicek01@upol.cz
†Electronic address: bartkiewicz@jointlab.upol.cz
‡Electronic address: antonin.cernoch@upol.cz
§Electronic address: k.lemr@upol.cz

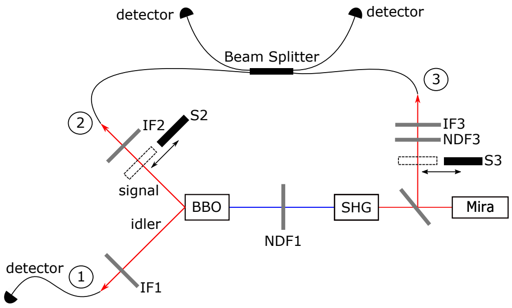

FIG. 1: Setup of the experiment, 1 – idler mode, 2 – signal mode, 3 – attenuated fundamental laser mode, IF(1-3) – interference filters (3 nm in FWHM), NDF(1,3) – neutral density filter, S(2,3) – shutters, SHG – second harmonics generation, Mira – Ti-sapphire fs laser (central wavelength of 826 nm, FWHM of 11 nm), BBO – a β-BaB_2O_4 crystal for SPDC.

monochromatic, but for each wavelength from their spectrum the following reasoning holds. Let us denote $|\psi_s\rangle$ the state of signal and idler modes of the SPDC generated photons (Nos. 1 and 2) and $|\alpha\rangle$ the coherent state of the attenuated fundamental laser mode (No. 3). We start with the Hamiltonian for SPDC process in the form of [31]

$$\hat{H}_{\mathrm{SPDC}} = \gamma\alpha_p \hat{a}_1^\dagger \hat{a}_2^\dagger + h.c., \tag{1}$$

where $\gamma \ll 1$ is an interaction constant, α_p is a strong pumping amplitude of frequency doubled laser beam and $\hat{a}_1^\dagger$, $\hat{a}_2^\dagger$ are creation operators of the idler and signal photon modes respectively. The corresponding evolution operator is then of the form of

$$\hat{U} = \exp\left(\frac{i}{\hbar}\hat{H}t\right). \tag{2}$$

The state of the signal and idler modes is obtained by applying the $\hat{U}$ operator to the initial vacuum state

$$|\psi_s\rangle \propto |00\rangle + \frac{it}{\hbar}\gamma\alpha_p|11\rangle + \frac{(it\gamma\alpha_p)^2}{2\hbar^2}|22\rangle + ... \tag{3}$$

We can express this state as

$$|\psi_s\rangle \propto |00\rangle + \kappa|11\rangle + \frac{\kappa^2}{2}|22\rangle, \tag{4}$$

for $|\kappa| \ll 1$ and

$$\kappa = \frac{it}{\hbar}\gamma\alpha_p. \tag{5}$$

The term $|00\rangle$ in Eq. (4), can be omitted because the first photon works as a herald which means that if it does not get detected the measurement will not succeed. This is under the assumption of negligible dark counts. Furthermore, we have to take into account probability of coupling the photons from SPDC into optical fibers. Let us denote t_1 and t_2 the amplitude coupling efficiency of idler and signal modes respectively. The state of the first and second photon then reads

$$\begin{aligned}|\psi_s\rangle \;&\propto\; 2\kappa t_1 t_2|11\rangle + 2\kappa t_1\sqrt{1-t_2^2}|10\rangle + \\ &+\; \kappa^2 t_1\sqrt{1-t_1^2}t_2^2|12\rangle + \kappa^2 t_1^2 t_2^2|22\rangle,\end{aligned} \tag{6}$$

where again we have excluded the terms corresponding to the first mode being in a vacuum state. Moreover, the last term in Eq. (6) can be neglected with respect to the third term since in typical experimental setups $t_{1,2} \ll 1$.

Next, we can express the coherent state of attenuated fundamental laser mode of the same wavelength as the generated photon pairs in Fock basis and limit the expansion to first N terms

$$|\alpha\rangle \approx \sum_{n=0}^{N}\frac{\alpha^n}{\sqrt{n!}}|n\rangle. \tag{7}$$

Any filtering or coupling efficiency do not change the nature of the attenuated laser mode which remains in a coherent state with amplitude α already including all possible losses. Thus we do not need to consider its coupling efficiency like in the SPDC modes.

If the source were to be perfect, there should be precisely one photon in each of the three modes. Simultaneous detection of these photons corresponds to genuine coincidences denoted CC_g. In reality, SPDC-based sources yield also higer-photon-number contributions. On the beam splitter, these photons may split leading to three-photon detection even if there were no photons in the attenuated laser mode [see the third term in Eq. (6)]. These detections denoted CC_s contribute to added noise. Similar source of noise are higer photon-number contributions from the fundamental laser mode that again can split on the beam splitter resulting in parasitic detections CC_f. Using Eqs. (6) and (7) for $N = 3$, we can identify the generation probabilities of the genuine coincidences as well as of the two parasitic contributions

$$CC_g \propto |\kappa|^2|\alpha|^2 t_1^2 t_2^2, \tag{8}$$

$$CC_s \propto t_1^2 t_2^4 \frac{|\kappa|^4}{4}, \tag{9}$$

$$CC_f \propto |\kappa|^2 t_1^2 \left(\frac{|\alpha|^4}{2} + \frac{|\alpha|^6}{6}\right). \tag{10}$$

Note that in Eq. (9), we have assumed $1 - t_1^2 \approx 1$ and in Eq. (10) $1 - t_2^2 \approx 1$. These approximation are valid especially when one considers a linear–optical setup fed by the source which strongly diminishes the transmisivity due to technological losses (back–scattering, fiber coupling etc.)

The goal now is to maximize the signal-to-noise ratio defined as

$$\mathrm{SNR} \equiv \frac{CC_g}{CC_s + CC_f} = \frac{12|\alpha|^2 t_2^2}{3|\kappa|^2 t_2^4 + 6|\alpha|^4 + 2|\alpha|^6}. \tag{11}$$

In a typical setup as depicted in Fig. 1, there are two parameters that can easily be tuned: (i) amplitude of the attenuated fundamental laser mode α and (ii) SPDC pumping amplitude α_p. In subsequent analysis, we investigate the dependency of SNR on these two parameters.

First we look at SNR as function of α, which translates to the observed ratio R between coincidence rates CC_f and CC_s

$$R \equiv \frac{CC_f}{CC_s} = \frac{2|\alpha|^4}{|\kappa|^2 t_2^4} + \frac{2|\alpha|^6}{3|\kappa|^2 t_2^4} \approx \frac{2|\alpha|^4}{|\kappa|^2 t_2^4}. \tag{12}$$

We have omitted the second expansion term from CC_f because for typical levels of attenuation to single-photon level $|\alpha| \ll 1$. The signal-to-noise ratio can now be approximated as function of the parameter R

$$\mathrm{SNR} \approx \frac{2\sqrt{2R}}{|\kappa|(R+1)}. \tag{13}$$

One can now find optimal value of R by searching for maximum of this function. When $|\alpha| \ll 1$ holds, the optimal value of R is 1. For larger values of $|\alpha|$ the optimal R shifts to slightly lower values because the approximation in Eq. (12) does not longer apply. In an experiment, one should thus seek to balance the false coincidence rates from SPDC and from attenuated fundamental mode.

In the subsequent analysis, we assume that $|\alpha| \ll 1$ holds and fix the parameter R at its optimal value of 1. The Eq. (13) then simplifies into the form

$$\mathrm{SNR} = \frac{2\sqrt{2}}{|\kappa|}, \tag{14}$$

which can, with the help of Eqs. (8) and (12), be expressed in terms of the genuine coincidence rate CC_g

$$\mathrm{SNR} \propto \sqrt[3]{\frac{16 t_1^2 t_2^4}{CC_g}}. \tag{15}$$

One can now make two important conclusions towards the performance of the interferometer. Firstly, the SNR can only be increased by decreasing the value of $|\kappa|$ which means by lowering the SPDC pumping strength $|\alpha_P|$. Secondly, the obtained coincidence rate depends on the coupling efficiency of the signal and idler SPDC modes. Especially, it scales with the fourth power of the amplitude transmissvity of the signal mode (or second power of intensity transmissivity). For any given pumping strength, one can improve the overall coincidence rate by improving the coupling efficiencies. The SNR, however, can not be improved by this adjustment.

III. EXPERIMENTAL IMPLEMENTATION

We have subjected our model and the resulting conclusions to an experimental test. Our experimental setup is depicted in Fig. 1. The attenuated fundamental laser mode (mode No. 3) is obtained by splitting a small portion from the femtosecond pumping laser beam (Coherent Mira at 826 nm). It then passes through a neutral density filter (NDF3) and 3nm-wide interference filter (IF3) before been coupled into single-mode fiber.

The main laser beam enters second harmonics generation unit (SHG), where its wavelength becomes 413 nm. The beam then passes through a neutral density filter (NDF1) and enters a Type I cut BBO crystal (0.64 mm thick) which due to SPDC generates idler and signal photons (Nos. 1 and 2) respectively. The photons in signal mode then pass through a 3nm-wide interference filter (IF2). The photons in idler mode pass through a 10nm-wide interference filter (IF1). The two SPDC modes are then coupled into single-mode fibers, idler mode is directly lead to a single-photon detector unlike the modes 2 and 3 that are mixed in a 50:50 fiber coupler before being detected. The avalanche photodiode detectors with suitable electronics record three-fold coincidence detections. Coincidence detection window was set to 5 ns, less than the laser repetition period of approximately 12.5 ns. We set the temporal displacement between photons 2 and 3, so they do not overlap in the fiber coupler. Thus we prevent the effect of two-photon interference.

In our experiment, we performed all the testing measurements in three steps: (i) with the shutters S2 and S3 open we detect all three-fold coincidences CC_a which include CC_g and parasitic contributions from signal and attenuated fundamental laser mode CC_s and CC_f

$$CC_a = CC_g + CC_f + CC_s. \tag{16}$$

(ii) then we close shutter S3 and obtain three-fold coincedences only if there is more than one photon in signal mode, thus we measure parasitic coincidence rate CC_s. (iii) finally we close shutter S2, open S3 and therefore obtain three-fold coincedences only if there is more than one photon in attenuated fundamental laser mode – parasitic coincidence rate CC_f. Note that CC_g is obtained from Eq. (16) simply by subtracting CC_f and CC_s from CC_a. Each step took about 100 s and the entire three-step procedure was reapeted multiple times, thus we have avioded a bias caused by long-term laser power fluctuations.

First, we have experientially verified the dependence of SNR on α, hence as a function of R [see Eq. (13)]. The experiment consisted of measuring the coincidence rates for various values of R using the above-mentioned three steps. The parameter R was changed by modifying transmissivity of NDF3. Experimentally obtained values are summarized in Tab. I and visualized in Fig. 2 together with the theoretical fit based on Eq. (13). The dashed line shows a fit in which we limited the expansion in Eq. (7) to the first three terms, however it turns

SNR [dB]	parameter R
-6.222 ± 0.740	0.013 ± 0.004
-4.440 ± 0.432	0.030 ± 0.004
-3.010 ± 0.440	0.040 ± 0.006
-1.105 ± 0.388	0.080 ± 0.008
-0.530 ± 0.442	0.340 ± 0.021
-0.086 ± 0.392	1.130 ± 0.052
-2.201 ± 0.241	1.510 ± 0.057
-3.502 ± 0.667	3.290 ± 0.290
-6.434 ± 0.727	7.180 ± 0.680

TABLE I: Experimentaly observed data and their respective errors when investigating the dependence of SNR on the parameter R

out that the model is not accurate enough for $R \to 10$ (see Fig. 2). With growing contribution of parasitic coincidences from the attenuated fundamental laser mode CC_f, and thus also growing ratio R, higher terms in Eq. (7) can no longer be neglected and the approximation in Eq. (12) does no longer hold. The solid line which represents a model where we used the first four terms of the expansion, is accurate enough throughout the entire measured range of R. We went a step further and expended our model (represented in Fig. 2 by dash-dot line) to include the first five terms of the expansion. There is a slight but unsubstantial improvement to the previous case and thus we find the four-term expansion to be the optimum compromise between accuracy and complexity. To simplify the following experiments, we have set the attenuated laser beam power so that the approximation in Eq. (12) holds. This means setting R $\in [0.2; 1]$ which also coincides with the SNR maximum.

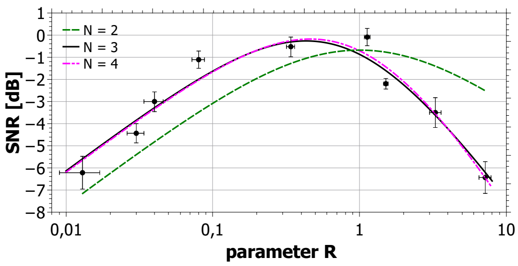

FIG. 2: Dependence of SNR on parameter R. Points visualize experimentally observed results. Lines correspond to various levels of expension in Eq. (7): to 2 (green dashed line), 3 (black solid line) and 4 (magneta dashed–dot line) terms.

As the next test, we have measured the dependence of SNR on the pumping amplitude α_p, which also translates into the dependence of SNR on the genuine coincidence rate CC_g [see Eqs. (14) and (15)]. We maintained the ratio R close to its optimum discovered in previous test ($R \approx 0.35 \pm 0.04$) and were changing α_p by changing

SNR [dB]	CC_g per 100 s	$P_p \propto \lvert\alpha_p\rvert^2$ [mW]
9.91 ± 1.274	2.91 ± 0.111	13 ± 2
7.50 ± 0.787	7.23 ± 0.217	25 ± 2
6.23 ± 0.714	19.88 ± 0.613	50 ± 2
5.17 ± 0.559	51.59 ± 1.384	104 ± 3
3.33 ± 0.577	135.28 ± 4.392	190 ± 3

TABLE II: Experimentally observed data and their respective errors when investigating the dependence of SNR on the CC_g and CC_g on the α_p.

transmissivity of NDF1. So for every measured value of SNR, we have adjusted both the NDF1 (influencing α_p) and NDF3 (to maintain constant R). The measurement procedure was also realised in the previously mentioned three acquisition steps. Experimentally obtained values are summarized in Tab. II and visualized in Fig. 3 together with a theoretical fit based on Eq. (14). The Fiq. 3 proves that our four-term model matches well the experimental data. We have also investigated dependence of CC_g on pumping power P_p which is proportional to pumping amplitude $|\alpha_p|^2$.

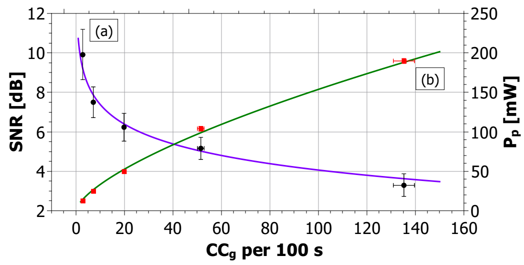

FIG. 3: (a) Dependence of SNR on genuine coincidence rate CC_g. Points visualize experimentally observed results, the solid violet line depicts fitted experimental data with theoretical dependence based on Eq. (14). (b) Dependence of CC_g on P_p. The solid green line depicts fitted experimental data with theoretical dependence based on Eq. (8).

The final two tests of our model involved verifying the dependence of genuine coincidence rate CC_g on the coupling efficiencies (i) t_1 and (ii) t_2 as predicted in Eq. (15). During each of the two tests, the parameter R and the pumping power were kept constant resulting in constant SNR. During the first test the value of SNR was (4.7 ± 1.6) dB. In the second test the SNR was (5.0 ± 1.3) dB. In order to test the dependence on idler and signal mode transmissivities t_1 and t_2, we have acquired the coincidences in the usual three steps for various levels of attenuation by closing a diaphragm on the idler and signal mode fiber couplers respectively. When the signal mode attenuation was set, the NDF3 in the attenuated fundamental laser mode was readjusted to maintain a constant R. This was not necessary when

idler attenuation (t_1)		signal attenuation (t_2)	
A_1	CC_g per 100 s	A_2	CC_g per 100 s
1	41.2 ± 3.2	1	44.8 ± 2.5
1.4	27.2 ± 1.7	1.3	22.2 ± 1.5
2	19.0 ± 1.7	1.9	10.0 ± 1
2.7	14.3 ± 1.8	2.8	6.2 ± 1
4	10.0 ± 1.7	3.8	2.3 ± 0.3

TABLE III: Experimentally observed data and their respective errors when investigating the dependence of CC_g on the attenuation factors A_1 and A_2.

closing the idler mode diaphragm. For better readability of our results, we introduce the idler and signal mode intensity attenuation factors A_1 and A_2 so that the modes' transmissivities become $t_j^2 \to t_j^2/A_j$ for $j = 1, 2$. Experimentally observed values are summarized in Tab. III and visualized in Fig. 4. Fig. 4 demonstrates that with constant SNR CC_g dependents on modes' transmissivities t_1^2 and t_2^2 as functions $\frac{1}{x}$ and $\frac{1}{x^2}$ respectively as predicted in Eq.(15).

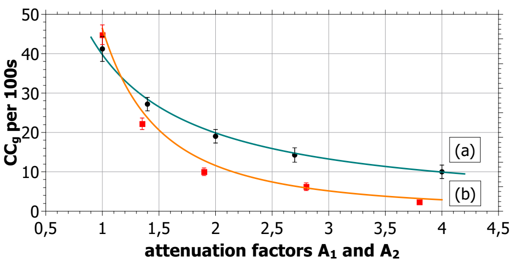

FIG. 4: (a) Dependence of CC_g on attenuation factor A_1. Points visualize experimentally observed results, the solid blue–green line depicts fitted experimental data with theoretical fit based on Eq. (15). (b) Dependence of CC_g on attenuation factor A_2. The solid orange line depicts fitted experimental data with theoretical dependence based on Eq. (15).

IV. IMPACT OF THE NOISE ON TELEPORTATION FIDELITY

We now investigate the impact of the above analyzed noise on quantum teleportation. Since quantum teleportation is a key ingredient in many quantum information protocols, it is essential to asses the influence of inherent noise of various photon sources on its performance. In quantum circuits, including teleporation, one often uses fidelity as a measure of the circuits quality. Assuming a pure input qubit state $|\psi\rangle_{in}$ and the resulting teleported state $\hat{\rho}_{out}$, fidelity can be calculated using the formula

$$F = |\langle\psi_{in}|\hat{\rho}|\psi_{in}\rangle|. \tag{17}$$

Note that when teleportation is replaced by classical "measure and recreate" protocol, the fidelity can not exceed its classical limit of $\frac{2}{3}$ [32]. Even though it is impossible to reach perfect fidelity $F = 1$ in realistic conditions, one still targets to maximize its value.

In our analysis we have calculated the dependence of average fidelity $\langle F\rangle$ on the signal-to-noise ratio (SNR). If we fix the parameter R to its optimum value ($R \approx 0.35$) the fidelity $\langle F\rangle$ is than a function that depends on CC_g and only one of the CC_s or CC_f since these two are bound by fixed parameter R. As a result the fidelity is a function of SNR. We have calculated the average fidelity using the formula

$$\langle F\rangle = \frac{P_{CC_g}F_g + P_{CC_s}F_s + P_{CC_f}F_f}{P_{CC_g} + P_{CC_s} + P_{CC_s}}, \tag{18}$$

where

$$P_{CC_g} = \frac{CC_g}{4f}, P_{CC_s} = \frac{CC_s}{4f}, P_{CC_f} = \frac{CC_f}{4f}, \tag{19}$$

are the probabilities of the coincidence events. f stands for the repetition rate of the pumping laser and F_g, F_s, F_f are the teleportation fidelities if the coincidence CC_g, CC_s or CC_f occur respectively. The value of teleportation fidelity $F_g = 1$ because from the definition there is one photon in each mode so the teleportation succeeds perfectly, at least in principle. On the other hand, the teleportation fidelities F_s and F_f have values of $\frac{1}{2}$. First one because the two photons in signal mode are randomly projected onto Bell states uncorrelated with the teleported photon which is missing. The later because the two photons in attenuated laser mode are not correlated with the idler mode which is thus a mixed state.

Calculated values are summarized in Tab. IV and visualized in Fig. 5. We observe that the average fidelity drops only slightly with decreasing SNR, so the average fidelity is above 80% for SNR around 3 dB. However this does not take into account other experimental imperfections (such as two–photon overlap, polarization adjustments etc.) that combining with photon-number noise can lead to such a low fidelity that the protocol fails. The fidelity uncertainty intervals were calculated using a Monte–Carlo simulation based on poisson distribution of detected coincidences.

V. CONCLUSIONS

In conclusion, we have shown that our model fits the experimental data very well. We have demonstrated the role of the ratio R between the SPDC-based and attenuated fundamental-based false coincidences. We have also confirmed its optimal value being close to 1 depending

fidelity F	fidelity uncertainty interval	SNR [dB]
0.96	$\langle 0.93, 0.98 \rangle$	9.91 ± 1.27
0.94	$\langle 0.90, 0.96 \rangle$	7.50 ± 0.79
0.92	$\langle 0.86, 0.95 \rangle$	6.23 ± 0.71
0.89	$\langle 0.85, 0.91 \rangle$	5.17 ± 0.56
0.85	$\langle 0.83, 0.86 \rangle$	3.29 ± 0.58

TABLE IV: Calculated data and their respective errors when investigating the dependence of average fidelity F on the SNR.

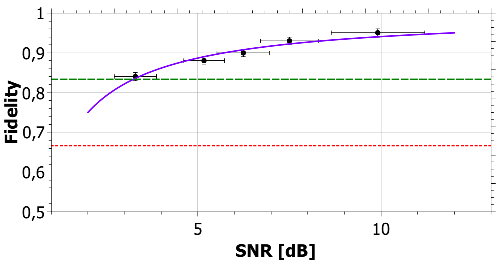

FIG. 5: Dependence of average fidelity $\langle F \rangle$ on SNR. Points visualize calculated results from experimentally observed SNRs. The solid violet line corresponds to our theoretical model, the dotted red line is the classical protocol limit ($F = 2/3$)[32] and the dashed green line indicates the secure teleportation, i.e., $F = 5/6$ cloning threshold see [30].

on the pumping strength. In the next step, we have verified that SNR (when optimal R) can only be increased by decreasing the SPDC pumping strength. Our data fit well both the SNR as a function of genuine coincidence rate, and also the predicted coincidence rate as a function of pumping strength. Finally, we have successfully tested the genuine coincidence rates as functions of coupling efficiencies while maintaining constant SNR. Our model and the obtained conclusions drawn from it can be useful for experimentalist when constructing a similar three-photon source and using it for teleportation-like protocols. With respect to that, we have made a prediction of the impact of this noise to teleportation fidelity. While fidelity drops smoothly with decreasing SNR, in conjunction with other experimental imperfections may lead to fidelity below the classical threshold.

Acknowledgement

Authors acknowledge financial support by the Czech Science Foundation under the project No. 17-10003S. KL and KB also acknowledge the financial support of the Polish National Science Centre under grant DEC-2013/11/D/ST2/02638. The authors also acknowledge the project No. LO1305 of the Ministry of Education, Youth and Sports of the Czech Republic financing the infrastructure of their workplace and VT also acknowledges the Palacky University internal grant No. IGA-PrF-2017-005

[1] G. Alber, T. Beth, M. Horodecki, P. Horodecki, R. Horodecki, M. Rötteler, H. Weinfurter, R. Werner, and A. Zeilinger, Quantum Information, Springer, Berlin, 2001, ISBN: 978-3-540-41666-1.

[2] M. Nielsen and I. Chuang, Quantum Computation and Quantum Information, Cambridge: Cambridge University Press, 2002, ISBN: 0-521-63235- 8.

[3] D. Bowmeester, A. Ekert, and A. Zeilinger, The Physics of Quantum Information, Springer, Berlin, 2000, ISBN: 978-3-642-08607-6.

[4] P. Kok, W. J. Munro, K. Nemoto, T. C. Ralph, J. P. Dowling, and G. J. Milburn, *"Linear optical quantum computing with photonic qubits,"* Rev. Mod. Phys. **79**, 135 (2007).

[5] X.-S. Ma, T. Herbst, T. Sheidl, *"Quantum teleportation over 143 kilometres using active feed-forward,"* Nature **489**, (2012)

[6] Q.-C. Sun, Y.-L. Mao, S.-J. Chen, W. Zhang, *"Quantum teleportation with independent sources and prior entanglement distribution over a network,"* Nature Photonics **10**, 671–675 (2016).

[7] C. Benett, G. Brassard, C. Crépeau, R. Jozsa, A. Peres, and W. Wooters, *"Teleporting an Unknown Quantum State via Dual Classical and Einstein- Podolsky-Rosen Channels,"* Phys. Rev. Lett. **70**, 1895 (1993).

[8] D. Bouwmeester, J. Pan, K. Mattle, M. Eibl, H.Weinfurter, and A. Zeilinger, *"Experimental quantum teleportation,"* Nature (London) **390**, 575 (1997).

[9] X.-S. Ma, S. Zotter, J. Kofler, R. Ursin, T. Jennewein, Č. Brukner and A. Zeilinger, *"Experimental delayed-choice entanglement swapping,"* Nature Physics **8**, 479–484 (2012).

[10] W. Tittel, J. Brendel, B. Gisin, T. Herzog, H. Zbinden, and N. Gisin, *"Experimental demonstration of quantum correlations over more than 10 km,"* Phys. Rev. A **57**, 3229 (1998).

[11] D. Gottesman, I. L. Chuang, *"Demonstrating the viability of universal quantum computation using teleportation and single-qubit operations,"* Nature **402**, 390-393 (1999).

[12] J. G. Rarity, P. R. Tapster and R. Loudon, *"Non-classical interference between independent sources,"* Journal of Optics B: Quantum and Semiclassical Optics **7** 1464 (2005).

[13] J.-W. Pan, Z.-B. Chen, C.-Y. Lu, H. Weinfurter, A. Zeilinger, and M. Żukowski,*"Multiphoton entanglement and interferometry,"* Rev. Mod. Phys. **84**, 777 (2012).

[14] T. Tashima, T. Wakatsuki, Ş. K. Özdemir, T. Yamamoto, M. Koashi, and N. Imoto, *"Local Transformation of Two Einstein-Podolsky-Rosen Photon Pairs into a Three-Photon W State,"* Phys. Rev. Lett. **102**, 130502 (2009).

[15] B. Lounis and M. Orrit, *"Single-photon sources,"* Reports on Progress in Physics **68** 0034-4885-R04 (2005).

[16] S. Scheel, *"Single-photon sources–an introduction,"* Journal of Modern Optics **56**(2-3) (2009).

[17] Z. Y.Ou and L. Mandel, *"Observation of spectral quantum beating with separated photodetectors,"* Phys. Rev. Lett. **61**, 54 (1988).

[18] K. Laiho, K. N. Cassemiro, and Ch. Silberhorn, *"Producing high fidelity single photons with optimal brightness via waveguided parametric down-conversion,"* Opt. Express **17**, 22823 (2009).

[19] R-B. Jin, J. Zhang, R. Shimizu, N. Matsuda, Y. Mitsumori, H. Kosaka, and K. Edamatsu, *"High-visibility nonclassical interference between intrinsically pure heralded single photons and photons from a weak coherent field,"* Phys. Rev. A **83**, 031805(R) (2011).

[20] G. Harder, V. Ansari, B. Brecht, T. Dirmeier, Ch. Marquardt, and Ch. Silberhorn, *"An optimized photon pair source for quantum circuits,"* Opt. Express **21**, 13975 (2013).

[21] N. Bruno, A. Martin, R. T. Thew, *"Generation of tunable wavelength coherent states and heralded single photons for quantum optics applications,"* Opt. Comm. **327**, 17 (2014).

[22] R-Bo. Jin, T. Gerrits, M. Fujiwara, R. Wakabayashi, T. Yamashita, S. Miki, H. Terai, R. Shimizu, M. Takeoka, and M. Sasaki, *"Spectrally resolved Hong-Ou-Mandel interference between independent photon sources,"* Opt. Express **23**, 28836 (2015).

[23] M. M. Weston, H. M. Chrzanowski, S. Wollmann, A. Boston, J. Ho, L. K. Shalm, V. B. Verma, M. S. Allman, S. W. Nam, R. B. Patel, S. Slussarenko, and G. J. Pryde, *"Efficient and pure femtosecond-pulse-length source of polarization-entangled photons,"* Opt. Express **24**, 10869 (2016).

[24] C. Vitelli, N. Spagnolo, L. Aparo, F. Sciarrino, E. Santamato, and L. Marrucci, *"Joining the quantum state of two photons into one,"* Nat. Photon. **7**, 521–526 (2013).

[25] K. Lemr, A.Černoch, J. Soubusta, K. Kieling, J. Eisert, and M. Dušek, *"Experimental implementation of the optimal linear-optical controlled phase gate,"* Phys. Rev. Lett. **106**, 13602 (2011).

[26] K. Lemr, K. Bartkiewicz, A. Černoch, M. Dušek, and J. Soubusta, *"Experimental Implementation of Optimal Linear-Optical Controlled-Unitary Gates,"* Phys. Rev. Lett. **106**, 153602 (2015).

[27] X.-L. Wang, L.-K. Chen, W. Li, *"Experimental Ten-Photon Entanglement,"* Phys. Rev. Lett. **117**, 210502 (2016).

[28] G. Brassard, N. Lütkenhaus, T. Mor, and B. C. Sanders, *"Limitations on Practical Quantum Cryptography,"* Phys. Rev. Lett. **85**, 1330 (2000).

[29] Y. Zhao, B. Q., X. Ma, H.-K. Lo, and L. Qian, *"Experimental Quantum Key Distribution with Decoy States,"* Phys. Rev. Lett. **96**, 070502 (2006).

[30] Ş. K. Özdemir, K. Bartkiewicz, Y.-X. Liu, A. Miranowicz, *"Teleportation of qubit states through dissipative channels: Conditions for surpassing the no-cloning limit,"* Phys. Rev. A **76**, 042325 (2007).

[31] M. H. Rubin, D. N. Klyshko, Y. H. Shih, A. V. Sergienko, *"Theory of two-photon entanglement in type-II optical parametric down-conversion,"* Phys. Rev. A **50**, 5122 (1994).

[32] S. Popescu, *"Bell's inequalities versus teleportation: What is nonlocality?,"* Phys. Rev. Lett. **72**, 797 (1994).